NASA Technical Paper 1005

An Analytical and Experimental Investigation of a 1.8 by 3.7 Meter Fresnel Lens Solar Concentrator

Leon J. Hastings, Steve L. Allums,
and Warren S. Jensen

AUGUST 1977

NASA

NASA Technical Paper 1005

An Analytical and Experimental Investigation of a 1.8 by 3.7 Meter Fresnel Lens Solar Concentrator

Leon J. Hastings, Steve L. Allums,
and Warren S. Jensen

George C. Marshall Space Flight Center
Marshall Space Flight Center, Alabama

NASA

National Aeronautics
and Space Administration

**Scientific and Technical
Information Office**

1977

TABLE OF CONTENTS

LIST OF ILLUSTRATIONS

LIST OF ILLUSTRATIONS (Continued)

LIST OF ILLUSTRATIONS (Concluded)

LIST OF TABLES

NOMENCLATURE

Symbol	Definition
cp	specific heat at bulk fluid temperature
D_i	tube internal diameter
h_i	internal heat transfer coefficient
I	incident direct solar flux
k	thermal conductivity at bulk fluid temperature
$\dot{m}$	fluid mass flowrate
Pr	Prandtl number, $\mu\, c_p/k$
Re	Reynolds number, $\rho VD/\mu$
ΔT	temperature difference
μ_b	absolute viscosity at bulk fluid temperature
μ_w	absolute viscosity at fluid film (wall) temperature
ρ	density at bulk fluid temperature

AN ANALYTICAL AND EXPERIMENTAL INVESTIGATION OF A 1.8 BY 3.7 METER FRESNEL LENS SOLAR CONCENTRATOR

I. INTRODUCTION

Activities at and sponsored by the Marshall Space Flight Center (MSFC) have been in progress to establish a technical data base on line-focusing acrylic Fresnel lenses that can generate temperatures in the 200° to 370°C. Compared to other concentration concepts, the technique is relatively unexplored; however, the acrylic lens is adaptable to mass production techniques by casting and/or calendering-extrusion processes which permit relatively low manufacturing costs [1]. The durability and weatherability of acrylic [2] and the ease of cleaning are other desirable qualities.

Initial phases of the Fresnel lens concept development were devoted to definition of lens optical performance. A simplified analytical model was developed by Ball State University and utilized in performance sensitivity studies [3]. A "grooves-down" lens configuration, as opposed to grooves toward the Sun, with an f-number of one was indicated to be optimum from a transmittance and concentration profile standpoint. Subsequently, the analytical model for the grooves-down geometry was refined and used in conjunction with experimentation to further define optical performance characteristics [4]. The experimentation was performed with a 56 cm wide, f-1, acrylic lens. The effort reported herein extends these earlier investigations to the testing and analysis of a full-scale lens, 1.83 by 3.66 m. The two principal objectives of the present phase were to (1) define the solar transmission and focusing characteristics of the lens, i.e., its optical performance and (2) utilize the lens in the solar collection mode by interfacing it with a receiver assembly.

II. LENS APPLICATION BACKGROUND

Initial goals of the MSFC concentrator effort were directed toward electrical power generation in the 100 to 10 000 kWe range with the distributed collector approach. As the program progressed, it became less system oriented

and centered on the development of a concentrator collector subsystem concept that could meet the general application requirement of thermal energy delivery within the 200° to 370°C range. Application to electrical power generation, commercial cooling, and industrial process heat are discussed in the following paragraphs.

For electrical power generation, a turbine inlet temperature of 282°C (540°F) was baselined as an interface requirement. Referring to Table 1, the 282°C inlet temperature represents a class of commercially available turbines presently utilized at levels from 100 kWe to 1000 MWe (Brown's Ferry nuclear power plant, for example) and is an achievable goal for distributed concentrator collectors. The system flow diagram is depicted in Figure 1. The collection loop concentrates/collects solar energy in a single phase transport fluid and

TABLE 1. BASELINE TURBINE INTERFACE CONDITIONS

Parameter	Power Level	
	100 kWe	100 MWe
Inlet Temperature	282° C (540° F)	282° C (540° F)
Inlet Pressure	310 N/cm^2 (450 psig)	655 N/cm^2 (950 psig)
Exhaust Temperature	50° C (122° F)	50° C (122° F)
Exhaust Pressure	1.23 N/cm^2 (1.79 psia)	1.23 N/cm^2 (1.79 psia)
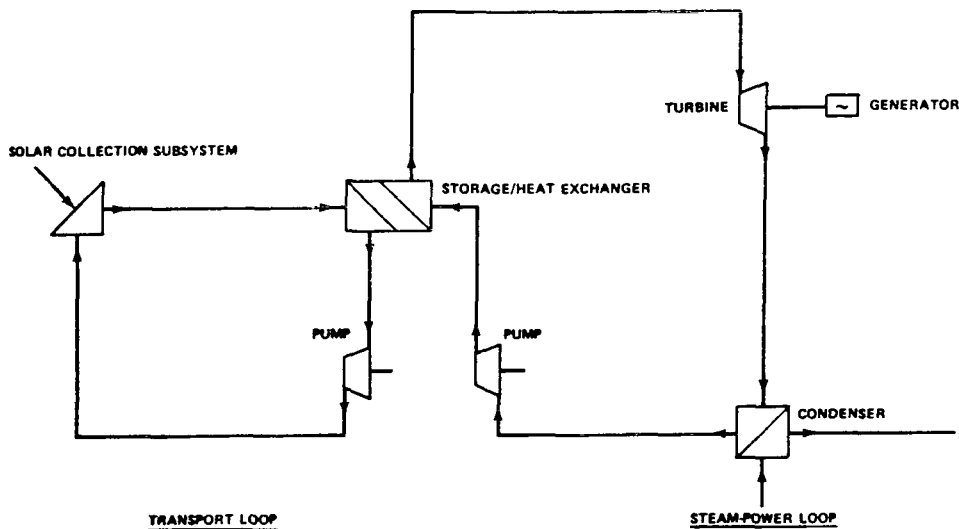
Figure 1. Solar thermal power plant flow schematic.

delivers it to the storage/heat exchanger site. The storage/heat exchanger, in turn, provides energy sufficient to generate steam at the required turbine inlet conditions in the steam/water transport loop. The two-loop type arrangement is similar to that used in nuclear plants and enables development flexibility in the collection loop without the complexities associated with two-phase fluid flow/heat transfer.

Figure 2 depicts some of the basic considerations involved in the development of solar cooling systems. Presently, solar cooling is performed using flat plate collectors and/or low level concentrators to interface with vapor absorption cooling cycles. However, the absorption cycle is limited to a COP (coefficient of performance) of 0.6. Auxiliary energy (heat) is also subject to the COP of 0.6 because it must pass through the absorption cycle. Therefore, if the auxiliary energy exceeds 25 percent of the total energy input, no energy savings occur relative to that of a conventional cooling system (COP = 2.5). The utilization of Rankine/vapor compression cooling cycles at flat plate solar collector temperatures is attractive since it allows mechanical auxiliary addition at a COP of 2.5. However, the solar system cooling performance is still limited to a COP of 0.6 due to low operating temperatures. Finally, solar collection at temperatures in the 230° to 285°C range, i.e., with solar concentrators, enables the achievement of solar cooling COP levels of 1.5 and greater using conventional steam turbines and vapor compression. Additionally, the auxiliary energy can be added with a COP of 2.5. With the higher COP levels and collection efficiency, the collector area and storage volume can be reduced by factors of four and three, respectively.

According to a recent study [5], energy consumption in the industrial sector for production purposes represents 41 percent of the national energy used. Further, the direct use of fuels by industry for process steam alone comprises 17 percent of the national energy requirement and, thus, represents an area of strong potential for solar energy applications. Figure 3 describes the percentage of process steam requirements for various temperature ranges. Approximately 70 percent of the energy is required in the 125° to 250°C range, i.e., within the capability of the distributed concentrator concept.

In summary, Fresnel lenses offer a means of achieving the required concentration/temperature levels for application to electrical power generation, commercial cooling, and industrial process heat. Additionally, McDonnell Douglas Astronautics, Western Division, has recently performed detailed Fresnel lens collector design optimization/cost studies and testing. Costs of approximately $183/m² ($17/ft²) and $108/m² ($10/ft²) with and without installation, respectively, have been projected, based on a mass production status. Thus, the Fresnel lens is cost competitive with other concentrator approaches.
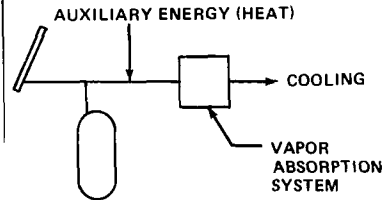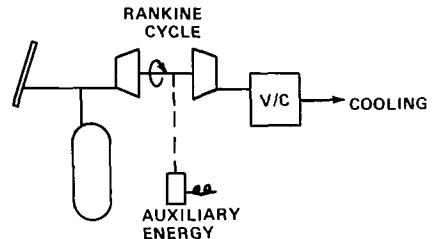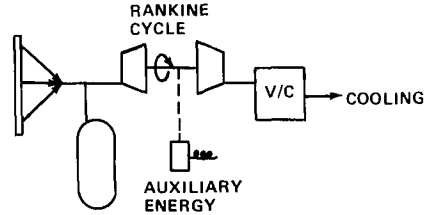
COOLING SYSTEM CONCEPT	OPERATING TEMP.	SYSTEM COP (COOLING OUT) (HEAT IN)	COLLECTOR EFFICIENCY	AUXILIARY ENERGY COP	COLLECTOR AREA	STORAGE VOLUME
FLAT PLATE/ABSORPTION	82°C (180°F)	.6	30%	.6	31 m^2 (333 ft^2)	2.27 m^3 (333 ft^2)
FLAT PLATE/VAPOR COMPRESSION	82 °C (180 °F)	.6	30%	2.5	31 m^2 (80 ft^2)	2.27 m^3 (600 gal)
FRESNEL LENS/VAPOR COMPRESSION	230-285 °C (450-550 °F)	1.5	50%	2.5	7.4 m^2 (600 gal)	.7 m^3 (185 gal)

Figure 2. Absorption and vapor compression solar cooling system comparison per ton of cooling.
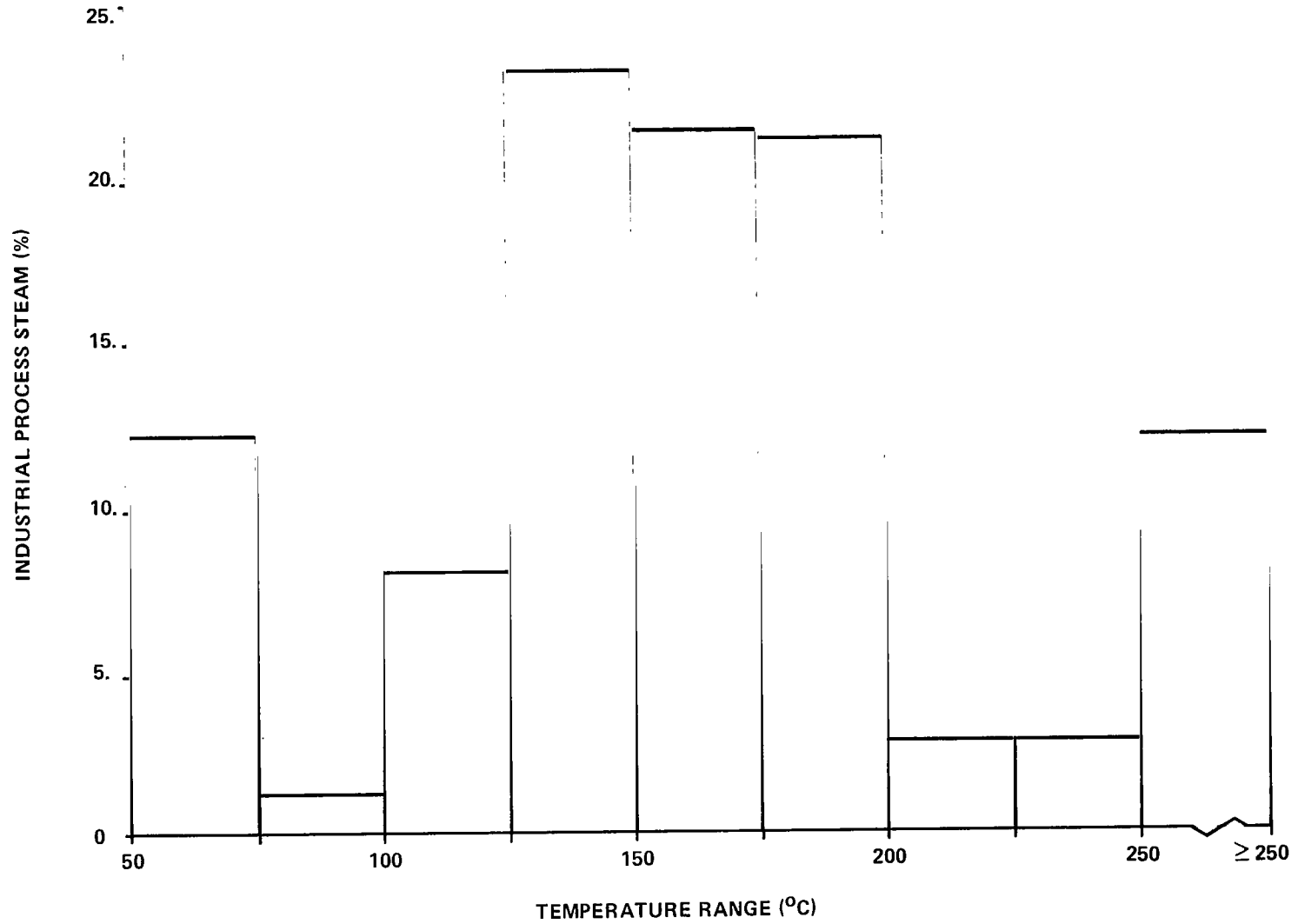
Figure 3. National industrial process steam requirements versus user temperature.

III. MAJOR TEST ARTICLE DESCRIPTION

A. General Description

The Fresnel lens test article[1] is described in Figures 4 and 5. The lens active aperture is 1.83 by 3.66 m (6 by 12 ft) and consists of an array of square panels. The lens tracks the Sun (two axis tracking) and focuses along a receiver assembly located approximately 1.68 m beneath the lens. The receiver assembly consists of a stainless steel absorber tube mounted in a reflecting trough or cavity. The tube is corrugated and coated with an absorptive coating to enhance its thermal performance. The transport fluid is Therminol 66, a single phase heat transfer medium by Monsanto Company. The transport loop consists of the expansion tank, pump, heater, absorber tube, and heat exchanger plus associated plumbing and controls. The fluid transport loop and test article are appropriately instrumented to measure collector performance characteristics for various test conditions. Controllable test parameters include fluid flowrate, receiver inlet fluid temperature, and Sun tracking accuracy.

Polyvinyl material forms an enclosure that includes the receiver assembly and bottom surface of the lens. The enclosure protects the grooved surface of the lens from dust and other contaminants and shields the collection tube assembly from direct atmospheric exposure, thereby minimizing contamination/degradation and thermal convection losses due to wind.

Further descriptions of the test article components and selection criteria are included in the subsequent sections.

B. Component Description

1. <u>Fresnel Lens</u>. The lens was assembled using two panel configurations which are identified as inside panels (those adjoining the lens axial centerline) and outside panels. Both types of panels have a 45.7 cm (18 in.) square aperture[2] with a 0.0635 cm (1/4 in.) border for mounting purposes. The lens

---

1. The test article structural and sun-tracking mechanism designs were provided by Messrs. C. Mueller and C. Heller of NASA-MSFC. Assembly of the test article components and a functional checkout were performed by Wyle Laboratories of Huntsville, Alabama.

2. The aperture size for each panel was restricted by manufacturing tooling limitations that existed in the U.S. when the panels were procured. Larger panels would be desirable and available in actual applications.

6
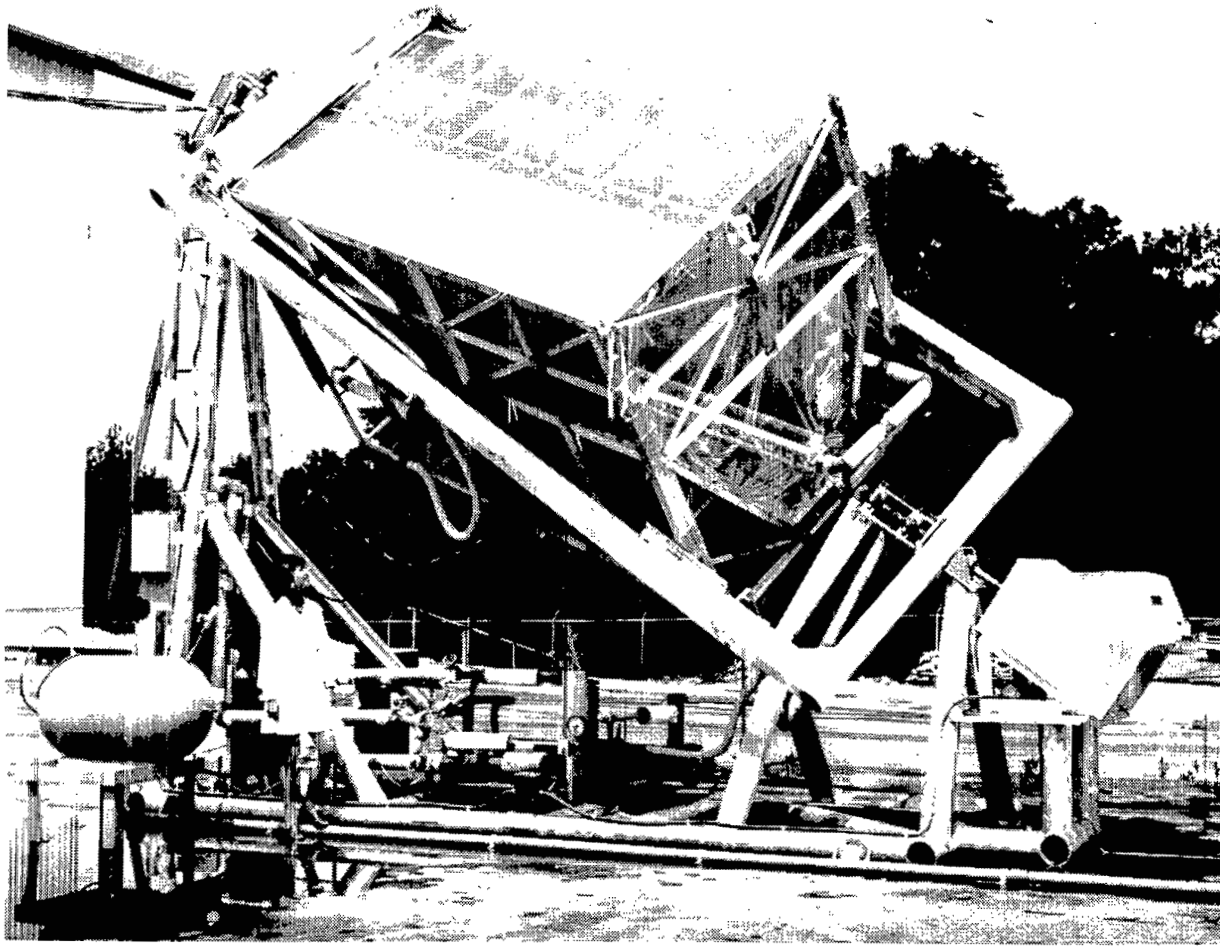
Figure 4. Fresnel lens test article photograph.

EXPANSION TANK

FRESNEL LENS

N

RECEIVER TUBE ASSEMBLY

SWIVEL JOINTS

SOLAR TRACKING
MECHANISM

HEAT EXCHANGER

FLUID CIRCULATION PUMP

S

HEATER
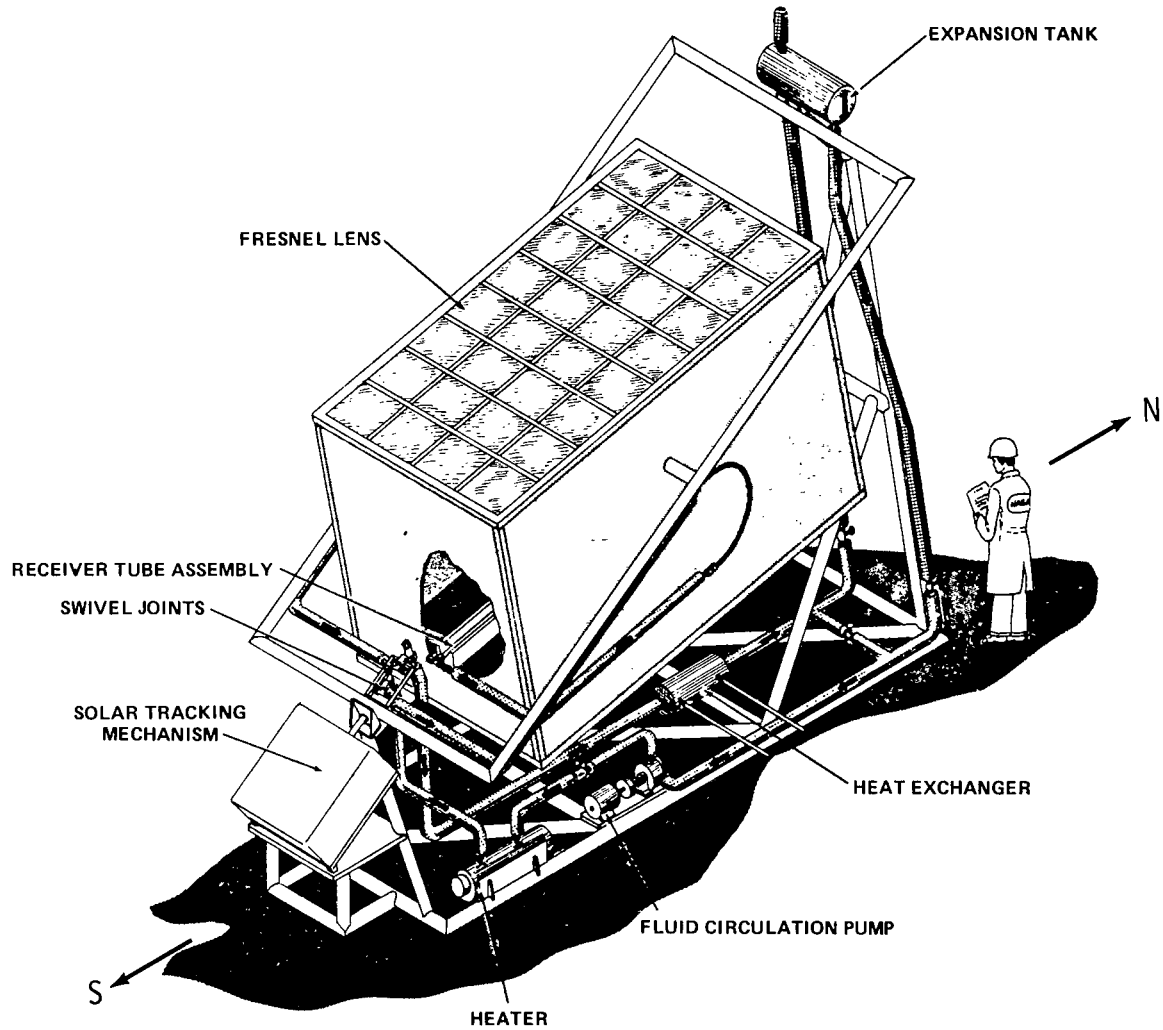
Figure 5.   Fresnel lens test article schematic.

geometry and characteristics are further defined in Figure 6 and Table 2. The panels were produced by Optical Sciences Group, Inc., (OSG) and represent the second set manufactured by OSG for solar concentration/collection test purposes. Experience derived from the first set, which formed a 56 cm lens [4], provided a basis for improving the manufacturing procedures.

The present lens was compression molded from Plexiglas V (811), a standard Rohm and Haas material. Plexiglas V (811)-100 UTV was originally specified because it has superior transmittance in the UV (ultraviolet) range (between 0.25 and 0.4 μ); however, it could not be procured in sheet form at the time the lens was to be fabricated. Apparently, though, the weatherability and aging characteristics of V (811) are quite good. Plexiglas 55, which is similar to V (811), was submitted to 17 years, 8 months of desert exposure in New Mexico and then evaluated to determine optical and mechanical property changes [2]. A transmittance degradation of approximately 7 percent occurred due to UV. Surface pitting by windblown sand caused an additional 3 percent loss. Similar aging characteristics are indicated by the manufacturers' data [6]. Since Plexiglas 55 and V (811) are UV absorbing formulations, less degradation would be expected with the UV transmitting formulations, e.g., Plexiglas II UVT. Thus, a 20 year lifetime is not an unrealistic expectation for acrylics. Further details on Plexiglas material properties and application recommendations are available from the manufacturer [6,7].

2. Receiver Assembly. The receiver assembly is described in Figure 7. The reflective cavity, which is constructed of anodized polished aluminum (ALZAK, Type I), has two functions. One is to aid in distributing the focused energy around the absorber tube, thereby minimizing problems associated with circumferential temperature gradients on the tube. Therefore, the energy is focused onto the cavity aperture rather than directly on the tube, i.e., the aperture is placed at the focal plane. Secondly, the reflective trough approach allows focusing on a target width (6.6 cm), larger than the tube diameter (1.9 cm), which minimizes transverse (E-W) Sun tracking deviation effects. The trough aperture is normally covered with a 0.005 cm Teflon FEP[3] transparent film. The receiver assembly length of 4.1 m (13.48 ft), which exceeds the lens length by 36.2 cm, was selected to allow the accommodation of longitudinal Sun tracking deviations of ±5.0°.

3. Tube Corrugation. The corrugated tube is a commercial product of the Wolverine Tube Division[4] of Universal Oil Products Company and is termed the Wolverine Korodense Tube, Type MHT. The tube was produced from

---

3. Trade name by DuPont.

4. Located in Decatur, Alabama.

OUTSIDE PANEL

INSIDE PANEL

47
(18.5 in.)

47
(18.5 in.)

A

A

B

B

GROOVE DIRECTION

GROOVE DIRECTION

13.23 GROOVES/cm

8.82 GROOVES/cm

− 0.635 cm (0.25 in.) BORDER
(TYPICAL ON ALL EDGES)

0.645

0.625

0.622

0.59

45.72
(APERTURE)

VIEW B–B

VIEW A–A

NOTES:

● DIMENSIONS IDENTICAL ON INSIDE AND OUTSIDE
   PANELS EXCEPT FOR GROOVE GEOMETRY

● GROOVES AND DIMENSIONS NOT TO SCALE

● ALL DIMENSIONS IN CENTIMETERS UNLESS NOTED OTHERWISE

Figure 6. Lens panel geometry.

TABLE 2. TEST LENS CHARACTERISTICS

Lens Type:	Cylindrical Fresnel, grooves down
Material:	Rohm and Haas Plexiglas V (811)
Fabrication Technique:	Compression molding
Manufacturer:	Optical Sciences Group, Inc.
Active Aperture:	182.9 cm (72 in.) wide 365.8 cm (144 in.) long
Total Aperture:	186.7 cm (73.5 in.) wide 374.6 cm (147.5 in.) long
Nominal Focal Length:	168.0 cm (66.15 in.)
Geometric f-number:	0.9 (based on total aperture)
Expected Transmission:	82 percent
Design Wavelength:	6250 Å

NOTE: Specifications provided by manufacturer.

stainless steel tube stock with a 1.91 cm (0.75 in.) O.D. and a 0.165 cm (0.065 in.) wall. A photograph and the corrugated tube geometry are presented in Figure 8. The axially spaced helical grooves on the outer wall and inwardly extending helical ridges on the inner wall give the tube a "corrugated" appearance. Shaping is performed without thinning the wall and the corrugated section O.D. does not exceed the O.D. of the original or "prime" tube.

Basically, the corrugations create a turbulating action on the inside of the tube, thereby reducing the laminar sublayer and increasing the heat transfer between the tube and internal fluid. Wolverine does not have experimental heat transfer data for temperatures exceeding 94°C. Until further data become available, the Wolverine suggested relation for determining the internal heat transfer coefficient, h_i, for conditions above 94°C is

$$\frac{h_i D_i}{k} = 0.15 \, (Re)^{0.7} \, (Pr)^{0.5} \qquad .$$
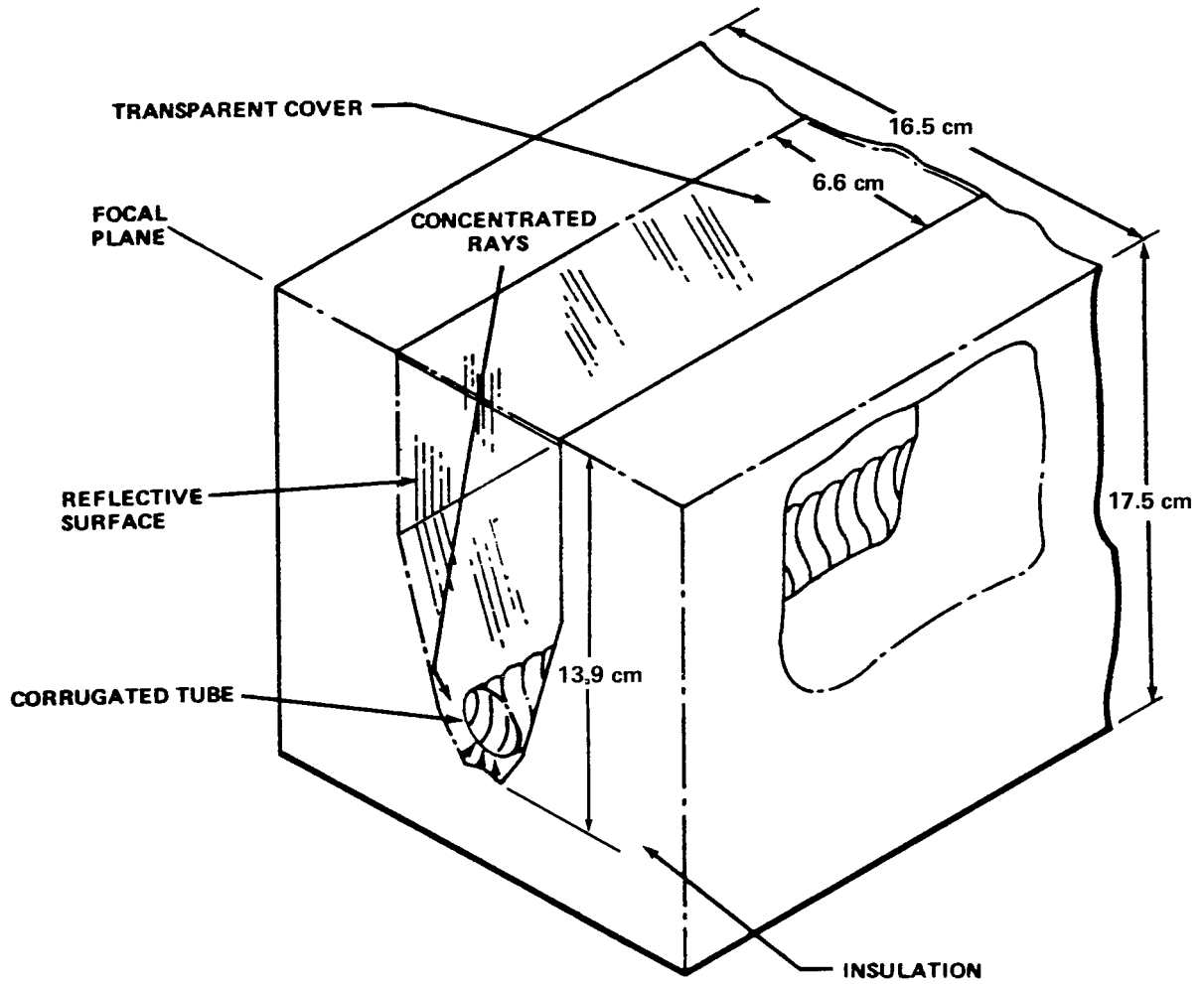
Figure 7. Receiver assembly description.

A corresponding standard smooth tube relation recommended by Monsanto [8] for Therminol fluids is

$$\frac{h_i D_i}{k} = 0.022 \, (Re)^{0.8} \, (Pr)^{0.4} \left(\frac{\mu_b}{\mu_w}\right)^{0.16}$$

Assuming identical Reynolds and Prandtl numbers for the smooth and corrugated tubes, then

CORRUGATED TUBE PHOTOGRAPH

CORRUGATION PITCH (1.054 cm)

PRIME TUBE
O.D. (1.91 cm)

CORRUGATED SECTION
O.D. (1.91 cm)

PRIME TUBE WALL (0.165 cm)

WALL AT CORRUGATION (0.165 cm)
CORRUGATION DEPTH (0.114 cm)
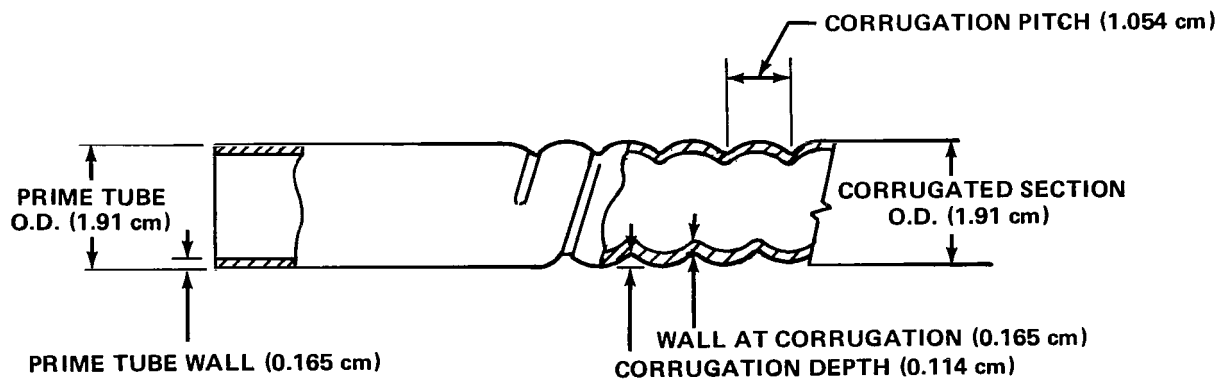
CORRUGATION GEOMETRY

Figure 8. Absorber tube corrugation.

$$\frac{h_i)_{\text{corrugated}}}{h_i)_{\text{smooth}}} = 6.82 \left(\frac{P_r}{R_e}\right)^{0.1} \left(\frac{\mu_w}{\mu_b}\right)^{0.16} .$$

For example, with 260°C Therminol 66 and an R_e of 5000, the corrugated to smooth tube coefficient ratio is 3.5. An an R_e of 10 000, the ratio becomes 3.4. Thus, the heat transfer increase is significant based on the Wolverine recommended relation.

The corrugated tubing pressure drop is increased relative to that with a smooth tube. As indicated by Figure 9, the corrugated tube friction factor is higher by three to five than that for a smooth tube at a given R_e number. Since the tube pressure drop is relatively small, the increased pressure loss appears to be an acceptable penalty for the increased thermal performance. For example, a pressure loss of approximately 0.034 atm (0.5 psi) is estimated for the present corrugated tube with a Thermonol 66 flow of 270 kg/hour at 260°C.
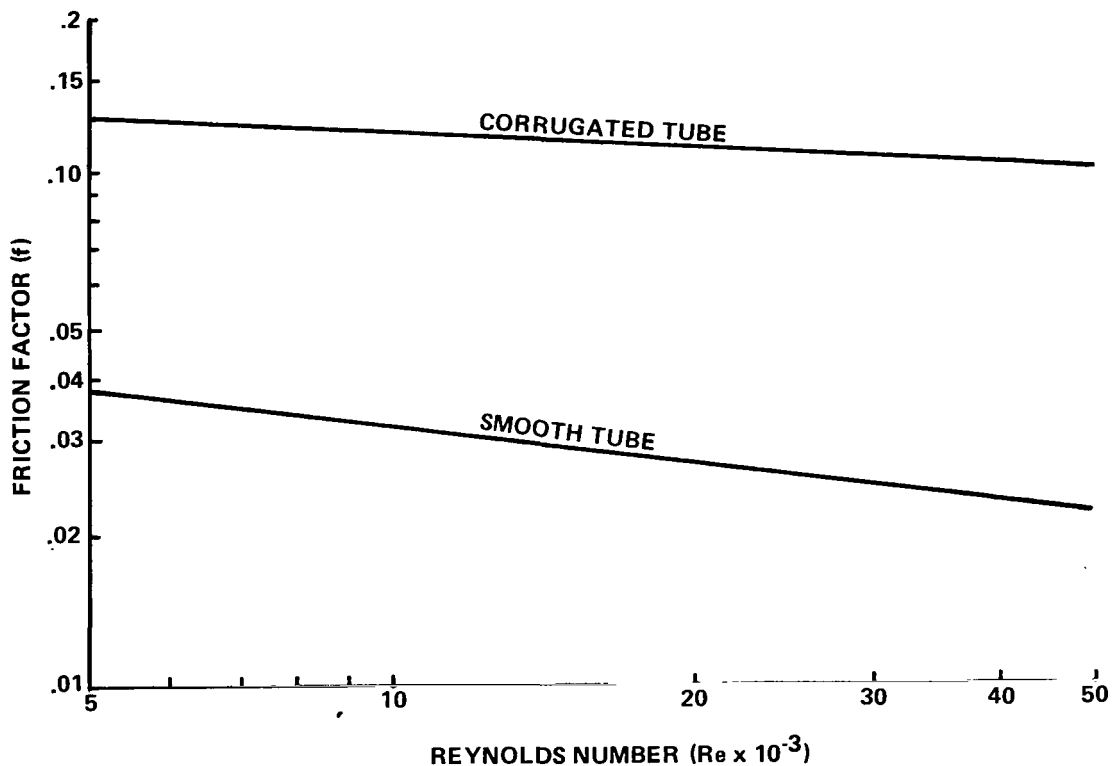
Figure 9. Corrugated tube friction factor.

4. Absorber Tube Coating. A program objective was to utilize a receiver assembly without an evacuated glass enclosure, realizing that thermal performance would be sacrificed somewhat for hardware simplification. Thus, the general requirements imposed on the tube absorptive coating were: thermal cycling at temperatures to 540°C without degradation, tolerance of atmospheric moisture, ease of application, and ease of handling/maintenance. Based on these constraints and preliminary tests, a "thermal oxide" type coating[5] was baselined as an initial coating. Such coatings, composed primarily of iron, chromium, and nickel oxides, form on stainless steel surfaces when heat treated. Under controlled conditions, a durable coating that has a high solar absorptivity and a low infrared emittance can be formed. Various application procedures were experimentally explored and environmental testing was conducted on selected versions of the oxide type coating. Details concerning the coating development are presented in the Appendix. Basic conclusions of the coating study were:

a. Two forms of the oxide coating are applicable in solar concentrators. One is a natural thermal oxide formed directly on stainless steel surfaces. The other is a natural thermal oxide formed on a nickel substrate.

b. The stainless oxide and the nickel oxide are durable when subjected to humidity and salt spray, but the nickel substrate does provide more resistance.

c. No degradation due to thermal cycling was evidenced.

d. Although the nickel oxide coating was more desirable, the stainless oxide was utilized on the actual absorber tube because of size limitations on in-house chemical bath facilities.

e. The corrugated tube surface precluded direct measurement of the actual tube optical properties. Based on comparisons with smooth surface measurements, a solar absorptance of 0.87 to 0.89 and an emittance of approximately 0.10 were achieved.

f. The oxide durability, stability, and ease of application warrant consideration of its benefits in long term applications. Further development could improve its optical performance.

---

5. Messrs. M. H. Sharpe, M. L. Roberts, and A. C. Krupnick of NASA/MSFC selected the oxide coating concept and developed the coating application/performance data presented herein.

5. <u>Transport Fluid.</u> The transport fluid selection was based primarily on the criterion of single phase, low pressure heat transport at operating temperatures exceeding 316°C (600°F). Additional general considerations were: fluidity at ambient temperatures, thermal stability, toxicity, materials compatibility, and commercial availability and cost. Table 3 presents representative, commercially available high temperature organic heat transfer fluids and example properties. Therminol 88 and Dowtherm A have maximum bulk temperature tolerances of 427°C and 399°C, respectively. However, Therminol 88 begins to solidify below 145°C, whereas Dowtherm A solidifies at 12°C. Therminol 66 and Dowtherm G have application temperature ranges of -4° to 343°C and -11° to 343°C, respectively, and closely exhibit the overall desired characteristics. Therminol 60 and Mobiltherm 603 are representative of fluids that can be used at temperatures not exceeding 316°C. Therminol 60 and Mobiltherm 603 may be advantageous in cold climate regions where startup at low temperatures is required. Therminol 66 was selected for initial testing based on its properties and its current use by Sandia Laboratories in similar testing with parabolic mirrors [9]. Therminol 66 property variations with temperature are listed in Table 4. Dowtherm G is also considered a viable candidate and may be utilized at a later date.

Details on design and operational considerations for high temperature organic heat transfer fluids are summarized in Reference 10 and are available from the respective manufacturers. Therminol 66 [8,11] is typical of the organic thermal fluids in that an inert gaseous "blanket" is required to minimize fluid oxidation and contamination. Also, an expansion tank is required to accommodate the fluid volumetric change that occurs with temperature fluctuations. For example, the fluid specific volume increases 34 percent with a temperature rise from 38° to 343°C. The fluid loop provisions required to accommodate Therminol 66 and to interface with the Fresnel lens collector are described in the following section.

6. <u>Fluid System and Instrumentation.</u> The fluid transport loop and recorded instrumentation are illustrated in Figure 10. The fluid is pumped from the expansion tank to the heater, where it is heated to provide the desired absorber tube inlet temperature. Upon exiting the absorber tube, the fluid passes through the heat exchanger where it is cooled before entering the expansion tank. The expansion tank is pressurized with gaseous nitrogen (typically 2 atm, absolute) to provide an inert atmosphere and to prevent air leakage into the Therminol system. Also, the expansion tank is located at the highest position within the system to minimize vapor entrapment and to provide a positive pressure on the pump inlet.

16

TABLE 3. HIGH TEMPERATURE ORGANIC FLUIDS AND PROPERTIES

Thermal Parameters	Properties at 316°C (600°F)					
	Therminol 88	Dowtherm A	Therminol 66	Dowtherm G	Therminol 60	Mobiltherm 603
Vapor Pressure, Absolute (atm)	0.342	3.09	0.46	1.23	1.0	0.225
Specific Heat (kcal/kg°C)	0.554	0.58	0.63	0.54	0.64	0.76
Density (kg/m^3)	880	790	770	870	797	666
Viscosity (cp)	0.335	0.19	0.34	0.318	0.285	0.412
Thermal Conductivity (kcal/m hr °C)	0.098	0.090	0.092	0.103	0.094	0.096
Useable Temperature Range (°C)	149 to 427	13 to 399	−4 to 343	−11 to 343	−51 to 316	−26 to 316
Pour Point (°C)	145[a]	12[b]	−28	−28	−68	−7
Flash Point (°C)	191	116	180	152	154	193
Miscellaneous						
Composition	Mixed Terphenyls	Diphenyl–Diphenyl Oxide Eutectic	Hydrogenated Terphenyls	Di and Triaryl Ethers	Polyaromatic Compounds	High VI Paraffinic Oil
Toxicity	Nontoxic	Nontoxic	Nontoxic	Nontoxic	Nontoxic	Nontoxic
Corrosion	None	None	None	None	None	Copper

a. Melt point

b. Freeze point

TABLE 4. THERMINOL 66 PROPERTY VARIATIONS WITH TEMPERATURE

Temperature		Density		Specific Heat		Thermal Conductivity		Viscosity		Vapor Pressure (Absolute)	
°F	°C	lb/ft³	kg/m³	Btu/lb. °F	kcal/kg °C	Btu/ft hr °F	kcal/m hr °C	lbm/hr ft	c_P	psi	atm
0	-18	64.9	1040	0.320	0.320	0.0720	0.1072	150 000	6200		
50	10	63.6	1020	0.350	0.350	0.0711	0.1058	617	255		
100	38	62.4	1000	0.380	0.380	0.0703	0.1046	67.8	28.0		
150	66	60.9	975	0.405	0.405	0.0695	0.1034	23.6	9.75		
200	93	59.3	950	0.430	0.430	0.0687	0.1022	10.1	4.20	0.0019	—
250	121	58.0	930	0.455	0.455	0.0678	0.1008	5.86	2.42	—	—
300	149	56.8	910	0.480	0.480	0.0670	0.0997	3.75	1.55	0.0039	—
350	177	55.2	885	0.505	0.505	0.0662	0.0985	2.57	1.06	—	—
400	204	53.6	860	0.530	0.530	0.0653	0.0972	1.88	0.78	0.039	0.003
450	232	52.5	840	0.555	0.555	0.0645	0.0959	1.40	0.58	0.096	0.007
500	260	50.5	810	0.580	0.580	0.0637	0.0948	1.08	0.45	1.93	0.131
550	288	49.5	793	0.605	0.605	0.0628	0.0935	0.87	0.36	3.86	0.262
600	316	48.1	770	0.630	0.630	0.0620	0.0923	0.82	0.34	6.76	0.46
650[a]	343[a]	46.8	750	0.655	0.655	0.0613	0.0912	0.65	0.26	14.70	1.0
700	371	45.6	730	0.680	0.680	0.0605	0.0900	0.49	0.20	19.33	1.32

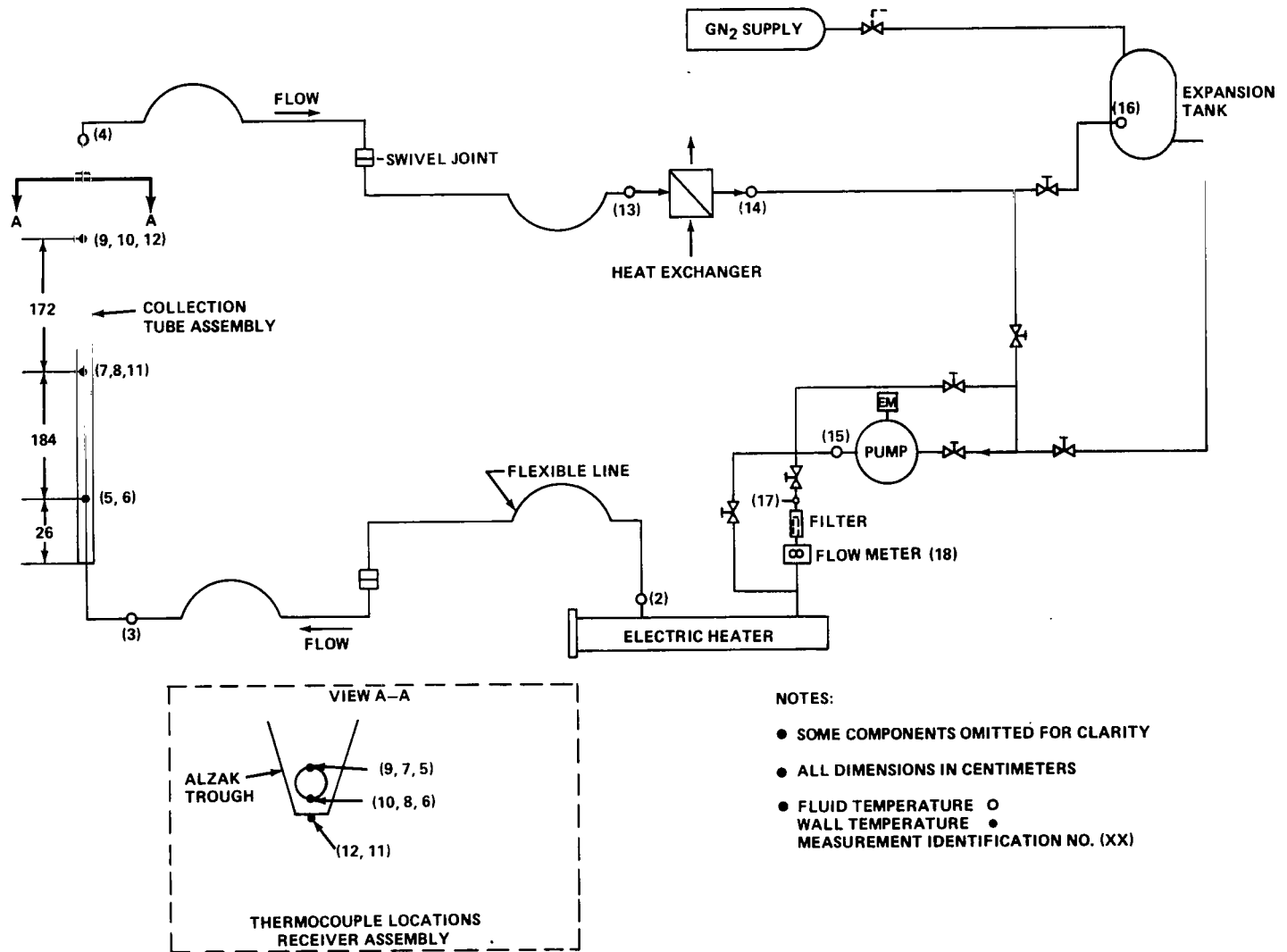a. Maximum recommended bulk temperature. The film temperature limit is 374°C (705°F).

Figure 10. Test article fluid flow loop.

Thus, the system was designed to control two basic test parameters, absorber tube inlet fluid temperature and flowrate. The flowrate can be varied between 0.95 and 4.9 liters/min (0.25 to 1.3 gpm) and the temperature from ambient to 316°C. A constant volumetric flow for a given fluid temperature is maintained by the positive displacement pump as verified with the flowmeter downstream of the pump. The flowmeter is a Fischer & Porter Company series 10C1512, 3/8-in. meter with a maximum capacity of 9.5 liters/min (2.56 gpm) and a rated accuracy of ±0.25 percent of the actual flowrate. The Chromalox 15 kW heater with its associated control system maintains selected heater outlet temperatures within ±0.2 percent. Selected absorber tube inlet temperatures are, in turn, maintained because the line between the heater outlet and tube inlet is insulated. The tube inlet and outlet fluid temperature measurement locations are upstream and downstream of the receiver assembly, respectively (Fig. 10). Negligible temperature differences occur between the tube interfaces and measurement locations because the lines are insulated.

Receiver assembly thermal characteristics are defined with additional temperature measurements. The longitudinal and circumferential temperature gradients on the absorber tube are measured using a pair of thermocouples at each of three longitudinal positions (Fig. 10). At each position, two thermocouples are mounted 180° apart, one on top of the tube and one on the bottom. Additionally, thermocouples are located on the backside bottom of the ALZAK reflective trough at two positions. Other instrumentation supporting the fluid transport system is that required for system monitoring, i.e., pump pressure, heat exchanger inlet/outlet temperatures, and expansion tank temperature and pressure.

Instrumentation external to the fluid loop includes an Eppley pyroheliometer (Model NIP) mounted on the lens frame, an ambient air temperature measurement, and five visual sight gauges for determining Sun alignment. A Sun alignment gauge was mounted at each of the four corners formed by the lens panel support structure and a fifth gauge on the structure just below the receiver assembly. The gauges were utilized to monitor Sun alignment of the entire tracking structure and any drift due to structural flexing or relaxation.

IV. TEST APPROACH

The general evaluation approach was to first establish the solar concentration or optical performance characteristics of the Fresnel lens using component bench testing and analytical modeling. The lens was then assembled in the full scale configuration and its optical performance checked to assess the impact of

the assembly process. Finally, when the lens was interfaced with the receiver assembly and operated in the solar collection mode, the lens and receiver influences on the total collection efficiency could be distinguished. Testing generally was conducted between 10:00 a.m. and 2:00 p.m. CST during cloudless periods to minimize variations in solar flux intensity. Significant atmospheric moisture haze which caused low, but steady, incident flux intensities was sometimes present.

A. Lens Performance Testing

Lens panels were experimentally evaluated at the component level using the test setup depicted in Figure 11. The Sun tracking heliostat provided a nonmoving Sun relative to the fixed Fresnel lens panels and is a gold first surface mirror, 118 cm in diameter. The Sun rays were controlled to within 4 arc sec of the perpendicular by the heliostat control sensors.

The baseline flux incident on the front of a lens was continuously measured during each test using an Eppley pyroheliometer. A photodiode sensor was translated across the image plane behind the lens to measure the lens concentration characteristics. The photodiode was calibrated against the pyroheliometer before each test series to assure compatibility of incident and focused energy measurements.

A reference or baseline concentration profile at the focal plane for perfectly positioned lens panels and the lens transmittance was first established. The reference data were then used to define deviations in imaging characteristics with various Sun lens orientation misalignments. Lens Sun tracking deviation data were obtained by tilting the lens at fixed angles relative to the reflected rays. After the panels were assembled to form the full scale lens/collector, the baseline concentration profile was again measured utilizing the same solar flux instrumentation used in the bench testing.

B. Collector Performance Testing

At the beginning of each test day, the lens surface was aligned perpendicular to the Sun using the visual sight gauges mounted on the tracking structural assembly. The alignment gauges were periodically monitored during the subsequent testing to assure that the proper lens Sun orientation was maintained. The procedure consisted of first establishing steady conditions at the selected flowrate and inlet temperature and, simultaneously, monitoring the pyroheliometer to

SUNLIGHT

PHOTODIODE SENSOR/TRANSLATION MECHANISM

SUPPORT FRAME

FRESNEL LENS PANELS

HELIOSTAT CONTROL AND
INCIDENT SOLAR FLUX SENSORS

MICRO-FLAT MARBLE TABLE

HELIOSTAT—GOLD FIRST-SURFACE
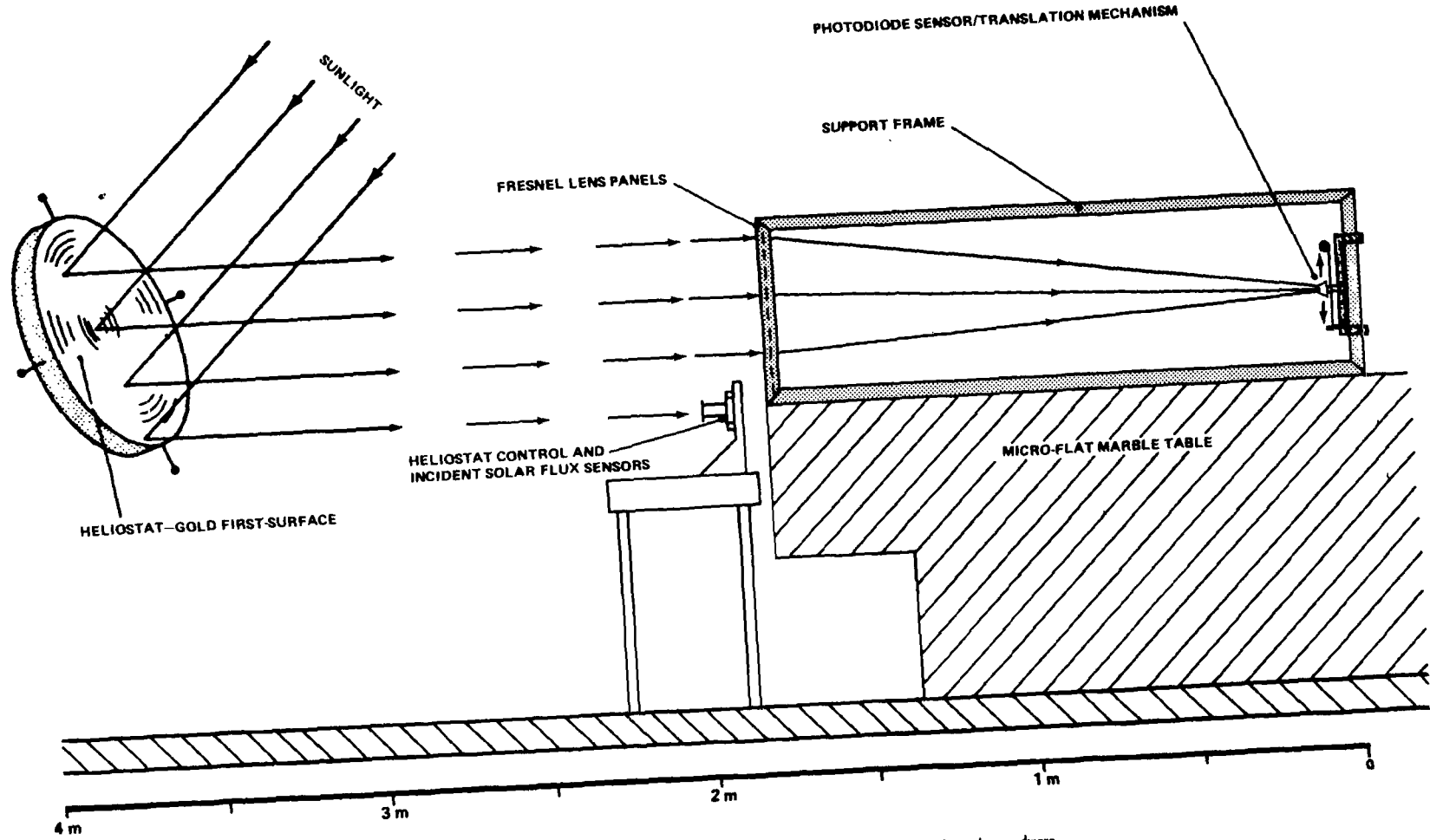
4 m   3 m   2 m   1 m   0

Figure 11. Lens panel optical performance test setup.

assure a constant direct solar flux input. Then, the data were recorded for periods ranging from 1 to 10 min. Subsequently, either the flowrate or inlet temperature was changed while maintaining the other variable as constant as possible, steady-state conditions were reestablished, and another data point was acquired. The recorded inlet to outlet temperature difference (ΔT) and mass flowrate were used to determine the collected energy ($\dot{m} c_p \Delta T$). The incident flux on the lens or "available energy" as measured by the pyroheliometer was then divided into the collected energy to determine the collection efficiency.

During the course of testing, additional test variables were introduced through hardware adjustments and modifications. The receiver assembly position relative to the lens was adjusted to defocus the trough aperture. Also, tests were conducted with and without the transparent FEP cover on the trough aperture. The lens surfaces were cleaned once, before the initiation of collector testing. The lens was not cleaned thereafter although the lens was usually covered when not in use to prevent accidental focusing.

V. LENS OPTICAL PERFORMANCE

A. Baseline Performance

The evaluation of parameters affecting lens performance required that a baseline solar concentration profile be established as a reference, preferably at the focal point. The focal point is defined as that position at which the lens design wavelength rays intersect beneath the lens. Thus, the actual focal length of a lens can best be located using a laser beam with the lens design wavelength. However, with the Sun as the source, a different approach had to be devised. Concentration profiles at various positions near the theoretical focal length were measured, and an optimum profile was selected based on maximum concentration and minimum target interception width.

The experimental focal plane position coincided with the theoretical focal length, i.e., 1.68 m (66 in.) from the lens front surface. The concentration profiles at the focal plane, or baseline profiles, measured in the bench tests and on the full scale test article are presented in Figure 12. Also shown is the profile computed by Ball State University using the analytical modeling technique previously presented [4]. The profile measured in the component tests indicated a peak concentration ratio of 67 with a 90 percent target width[6] of 4.2 cm. Profiles

---

6. A 90 percent target width represents the target size required to intercept 90 percent of that energy transmitted by the lens.
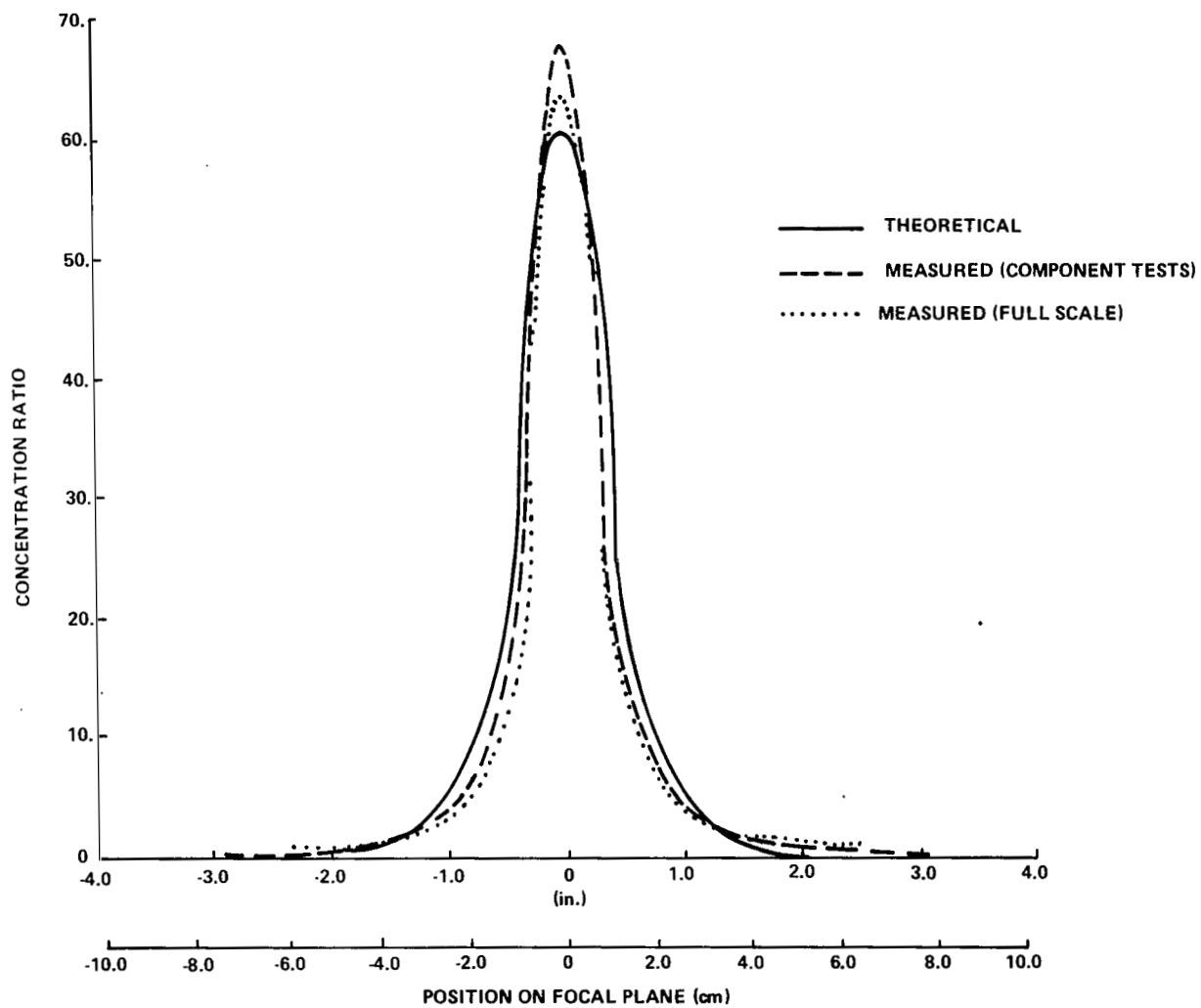
Figure 12. Analytical/experimental baseline concentration profiles.

measured on the full scale lens assembly correlated reasonably well with the bench test data. The full scale profiles did vary some with position along the receiver assembly due to a combination of slight structural misalignments inherent in supporting multiple panels and to experimental error.[7] The nominal peak concentration was 62 with a variation of ±3 percent; the 90 percent target width variation was ±8 percent from a nominal width of 5.0 cm. Approximately 95 percent of the energy transmitted by the lens was intercepted by the 6.6 cm trough aperture.

The analytical model resulted in a peak concentration of 61 and a 90 percent target width of 4.5 cm. Thus, the analytical and experimental profile correlation is considered to be good, although the analytical profile indicated a slightly higher transmittance. The measured and calculated transmittance versus serration position is presented in Figure 13. The computed and measured lens transmittances averaged 86 percent and 81 percent, respectively. The analytical/experimental data correlated well on the inside panels; however, the

Figure 13. Analytical/experimental transmission efficiency.

7. The full scale testing was more subject to experimental error than the component tests because of physical difficulties in instrumentation placement/ alignment.

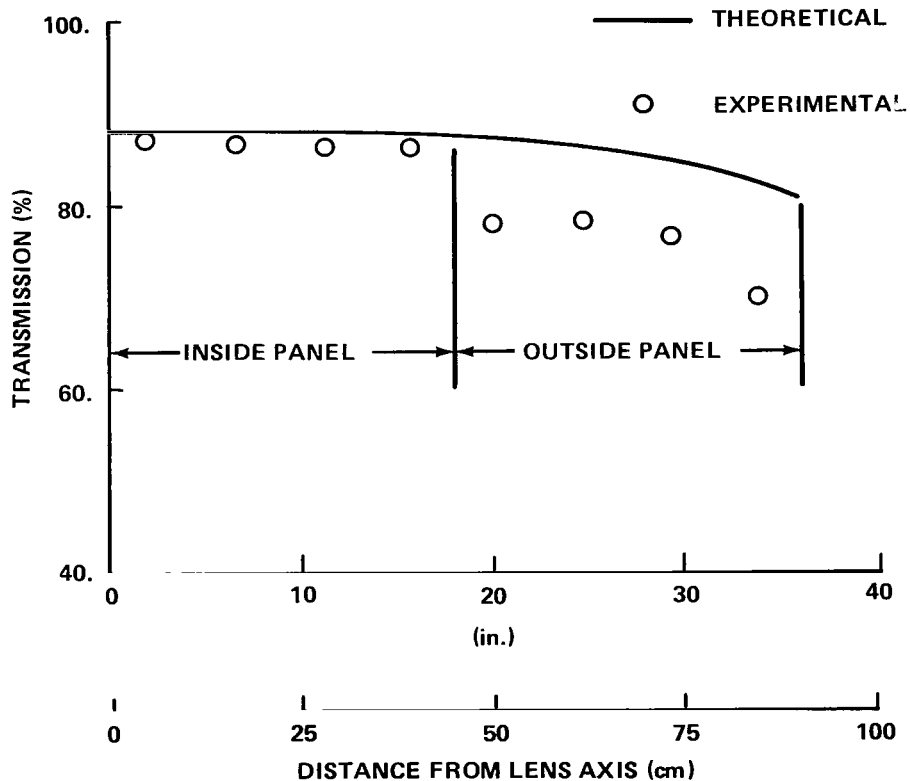outside panel data indicated an abrupt decrease in measured transmission efficiency. The transmission should not have varied significantly across the inside/outside panel interface. Based on the inside panel and previously measured transmittance data [4], modified manufacturing techniques should enable an increase in overall lens transmittance to the 85 to 86 percent level.

In conclusion, the overall lens performance was significantly improved relative to that previously measured with the 56 cm lens. Although the 1.83 m lens transmittance was approximately 7 percent lower than that obtained with the 56 cm lens, the larger lens produced less profile spreading, thereby enabling more reasonable target or receiver widths.

B. Transverse Alignment

Representative measured concentration profiles corresponding to transverse (E-W) Sun lens orientation deviations from 0.26°, 0.52°, and 0.75° are presented in Figure 14. A "no tracking error profile" is also presented for reference purposes. The general trends are much like those observed with the 56 cm lens, i.e., profile shifting, symmetry alteration, and peak concentration reduction at angles above 0.5°. Using the analytical techniques described in Reference 12, a profile for 0.75° misalignment was computed and is compared with that measured in Figure 15. The correlation is good considering the higher analytical transmittance.

The lateral shifting of the concentration profile is a primary influence on the target or receiver aperture width required for specific tracking accuracy tolerances. The 90 percent target widths required to accommodate the tracking deviations tested are specified in Figure 14; however, the target width dependence on the profile shift is more specifically illustrated in Figure 16 where target width increase and peak concentration shift versus tracking deviation are presented. The calculated target increase slightly exceeds that measured. Therefore, for design purposes a conservative approach would be to utilize the analytical data. Example measured and computed target width increases were 70 percent and 80 percent, respectively, at ±0.5°. The target increase can be predicted reasonably well by adding the peak position shift for a particular orientation to the baseline target width for angles up to approximately 1°. Above 1°, however, the profile skewness increases rapidly and begins to have a more pronounced effect on target width [12].

It is interesting to note that the peak concentration increased slightly at small angles and then began to decrease. The same trend was previously

26
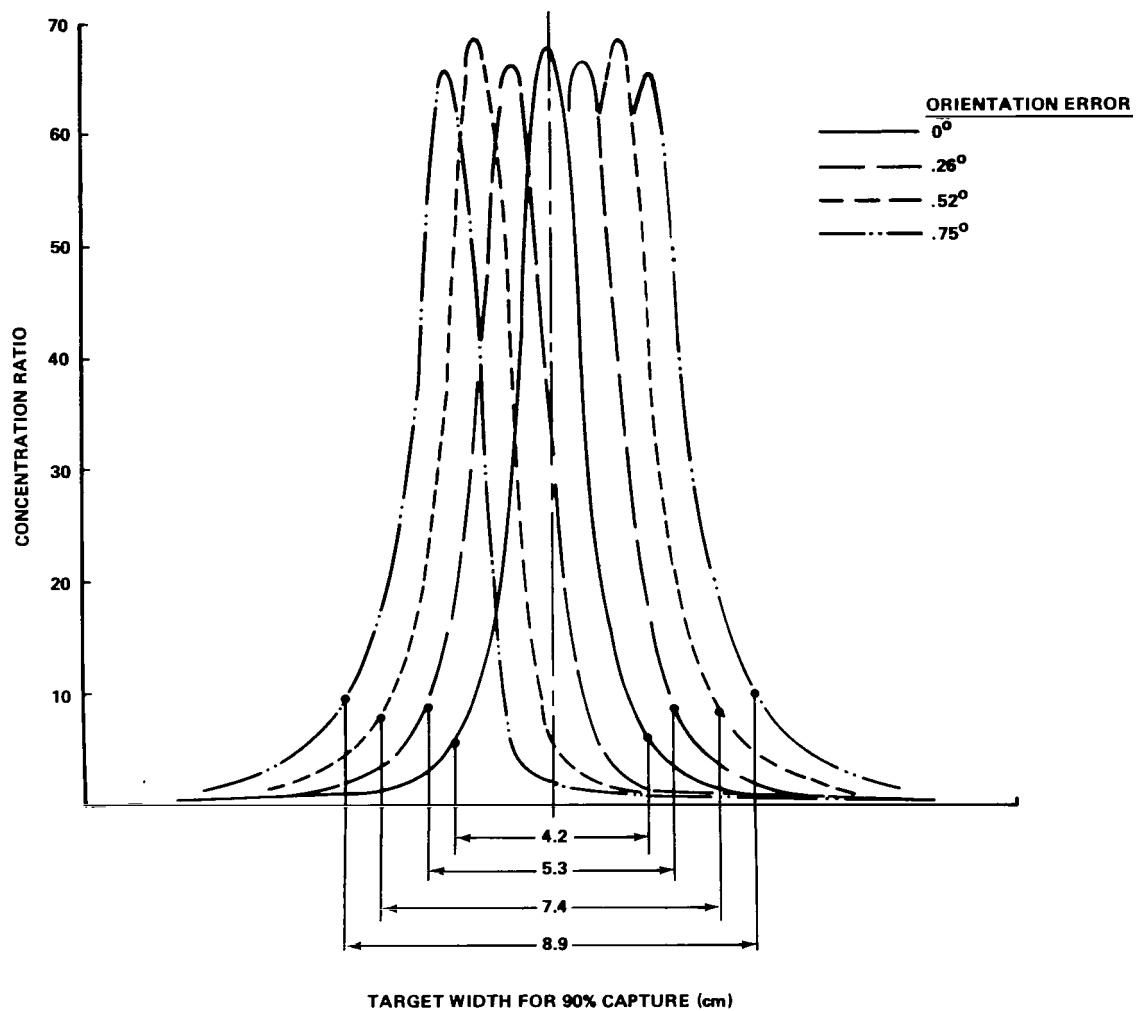
Figure 14. Measured transverse Sun alignment effects on concentration profile.

observed with the 56 cm lens and was initially thought to be an experimental error. However, the trend is apparently valid because it is also indicated in recent studies [12]. The measured and computed transmittance did not vary significantly with transverse misalignment.
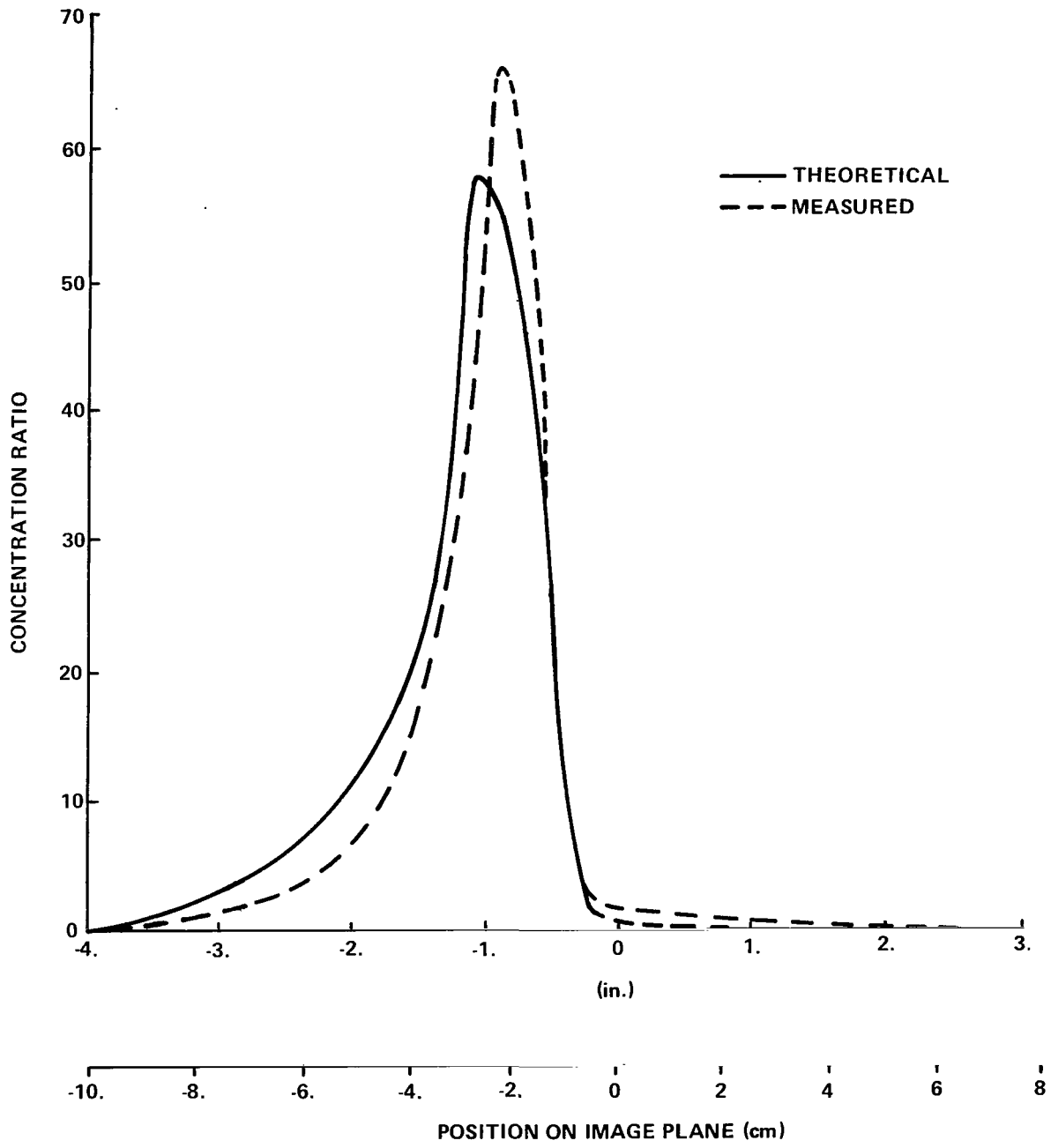
Figure 15. Analytical/experimental profiles with a 0.75° transverse
Sun alignment deviation.
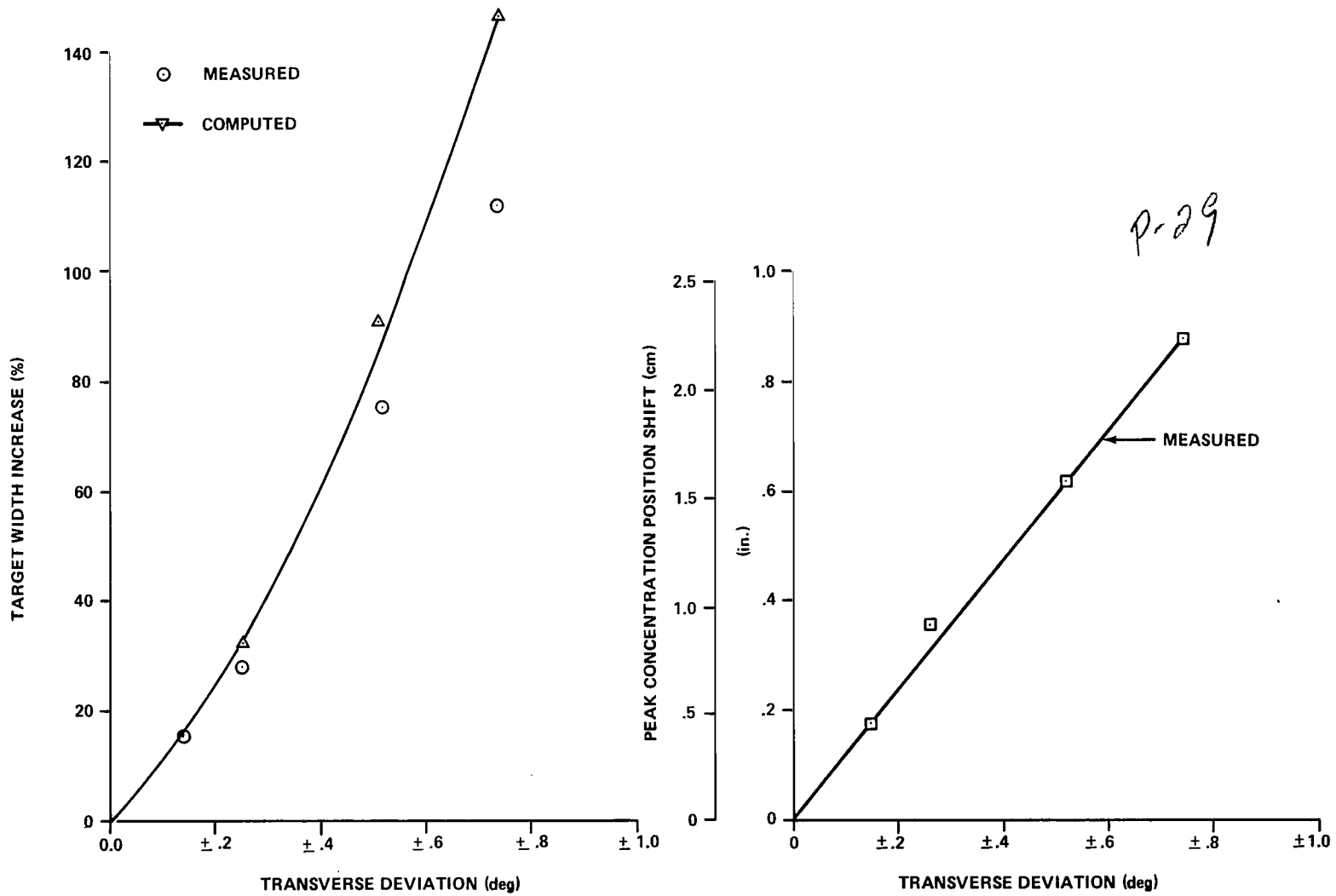
Figure 16. Transverse Sun alignment effects on target width and profile position.

C. Longitudinal Alignment

Sun alignment deviations in the longitudinal direction[8] from 1.5° to 9.5° were tested previously with the 56 cm lens. Because the lens performance was relatively insensitive to longitudinal alignment, detailed measurements of profile variations were not repeated with the present lens. Sun alignment deviations up to 6° were surveyed. Angles up to 5° had no significant effects on peak concentration or target width. Also, lens transmission was not significantly affected. Thus, the primary design consideration is that a collector receiver length must accommodate the profile shifting produced by longitudinal orientation deviations.

VI. COLLECTOR PERFORMANCE

Solar collection efficiencies and pertinent parameters were measured for a wide range of test conditions. The absorber tube flowrates were varied from 48 to 304 kg/hour and the inlet fluid temperatures from 100° to 295°C. Sun tracking errors up to 1.5° and 2° in the transverse and longitudinal direction, respectively, were also tested. The incident direct solar flux ranged from 470 to 900 W/m^2 (150-290 Btu/hr-ft^2). Ambient temperatures ranged from 26° to 34°C. Wind was not considered a significant factor because of the protected environment of the receiver assembly.

A. Performance Overview

The overall status of the collector performance testing is illustrated in Figure 17, which presents current and projected collection efficiencies versus average absorber tube fluid temperature. In accordance with the design approach, the receiver tube assembly was initially placed with the reflective cavity aperture at the focal plane. The collection efficiency ranged from 40 percent at 90°C to 21 percent at 300°C. An efficiency of approximately 40 percent at 300°C had been predicted. Based on the lens performance data previously discussed and visual observation, it was apparent that the energy was properly focused into the trough aperture by the lens. Further, it was noted that at a given fluid temperature the ALZAK temperatures were responsive to the magnitude of energy incident on the lens. Therefore, it was concluded that the reflective trough was not performing as expected. It is extimated that 55 percent of the energy was reflected by the ALZAK, whereas 80 percent was anticipated.

---

8. Longitudinal deviations are defined as those deviations occurring in the vertical plane containing the Sun and the receiver longitudinal axis.
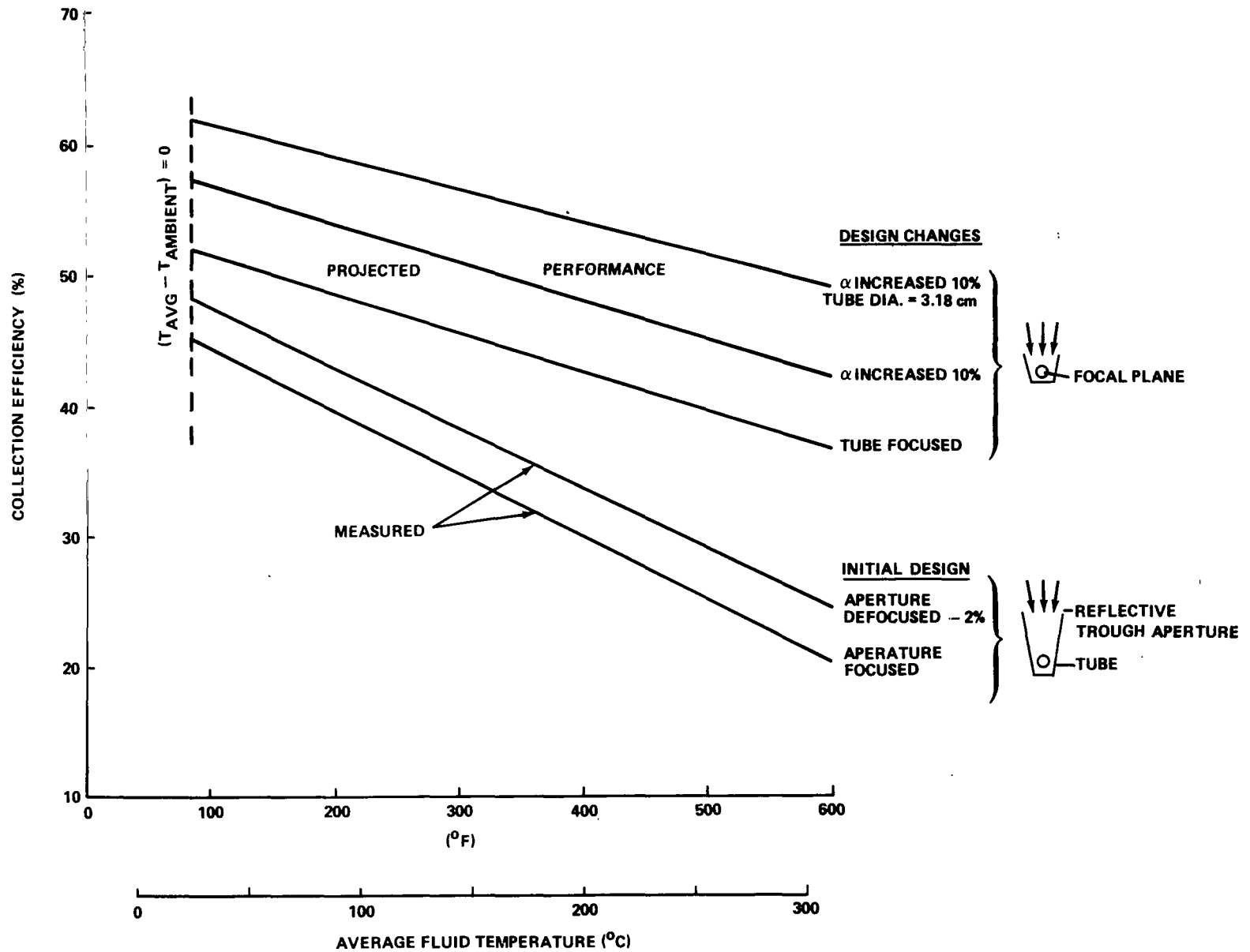
Figure 17. Fresnel lens collector performance overview.

These conclusions were further confirmed by moving the trough assembly 3.2 cm toward the lens such that the aperture was defocused approximately -2 percent. This move increased the energy directly impinging on the tube from approximately 21 percent to 34 percent and decreased the energy concentrated on the reflective surface from 75 to 55 percent. The "spillover" (energy focused outside the aperture) was increased from 4 to 11 percent, the maximum that could be tolerated. As indicated by Figure 17, the defocused conditions did result in a modest, but definite, performance improvement, e.g., increased from 21 to 26 percent at 300°C.

Future receiver assemblies will basically involve placement of the tube at the focal plane, thereby further increasing the energy directly focused on the tube surfaces. If a reflective surface is utilized, it will serve a backup rather than primary function. Increasing the tube absorptivity and diameter should enable an efficiency improvement to the 40 to 50 percent range at 300°C. An additional alternative is utilization of higher f-numbers to increase the transmittance and lower the receiver or target width, thereby increasing collection efficiency. Therefore, future testing will also address the influence of f-numbers greater than one.

B. Sun Tracking Deviation Effects

The influences on collection efficiency of Sun tracking deviations in the transverse (E-W) and longitudinal directions are illustrated in Figure 18. The transverse error data was measured with the trough aperture focused. Transverse deviations of 0.5° or less had no apparent effect on the collector performance since over 85 percent of the energy was still focused into the trough aperture. The energy spillover increased rapidly above 0.5° and the collection efficiency decreased accordingly. Longitudinal alignment deviations up to 2.0° were tested with no change in efficiency. Although the receiver assembly length was sized to tolerate a 5.0° deviation, support structure shadowing prevented testing at higher angles. Based on present and previous bench testing, 5.0° deviations should have no significant effects.

In conclusion, the Sun alignment effects on collection efficiency were consistent with the concentration profiles measured in the bench tests. It should be noted that the "transverse error versus efficiency data" is a strong function of receiver configuration. However, the longitudinal data have general application to other receiver designs, provided the receiver length is adequate to accommodate the changes in heated length that accompany longitudinal deviations.
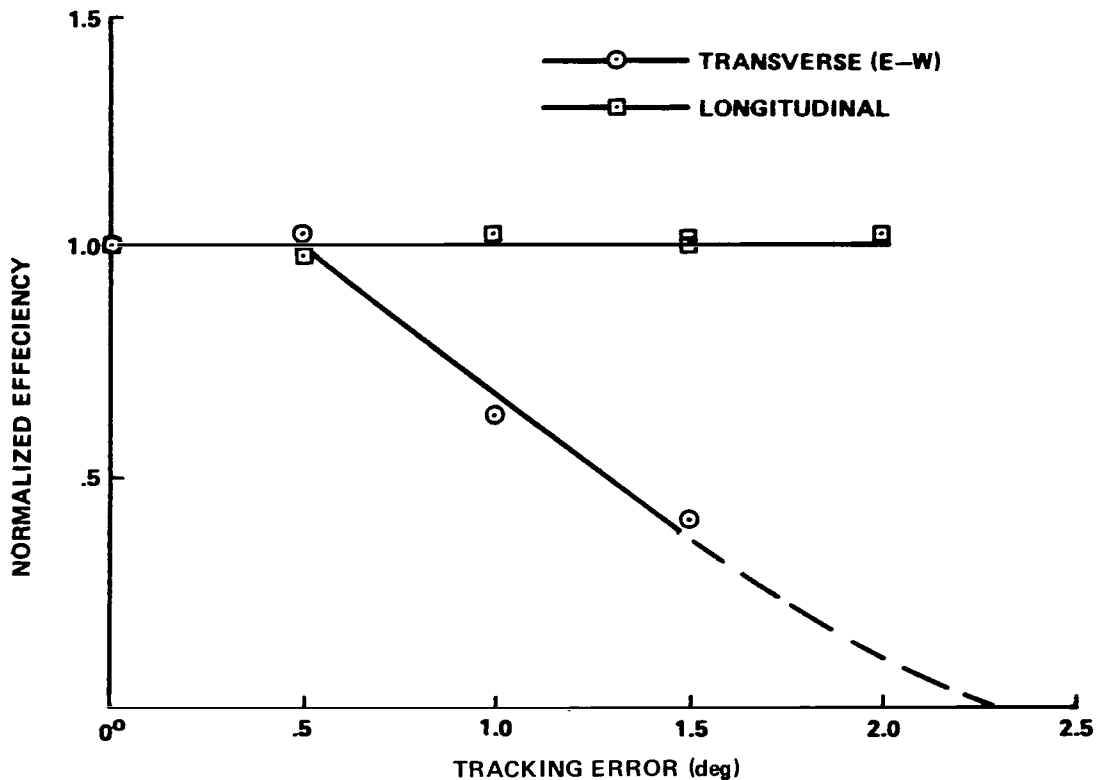
Figure 18. Transverse Sun alignment effects on measured
collector performance.

C. Miscellaneous Effects

Incident solar flux magnitude, transport fluid flowrate, and the presence/ removal of the FEP window were other parameters and effects evaluated. Collector performance trends with these parameters are discussed in the following paragraphs.

1. Solar Flux. The direct solar flux variations were less than ±16 percent during a given day, but ranged from 470 to 900 W/m^2 (150 to 287 $Btu/hr\text{-}ft^2$) over the 10 week test period. It was anticipated that the solar flux magnitude would have an effect on collection efficiency. However, when the standard data presentation format of "collector efficiency versus $\Delta T/I$"[9] was utilized, significant data scatter occurred, especially when data collected at various solar flux levels were compared. Figure 19 illustrates this effect using the defocused

9. ΔT is average fluid to ambient temperature difference and I is incident direct solar flux.
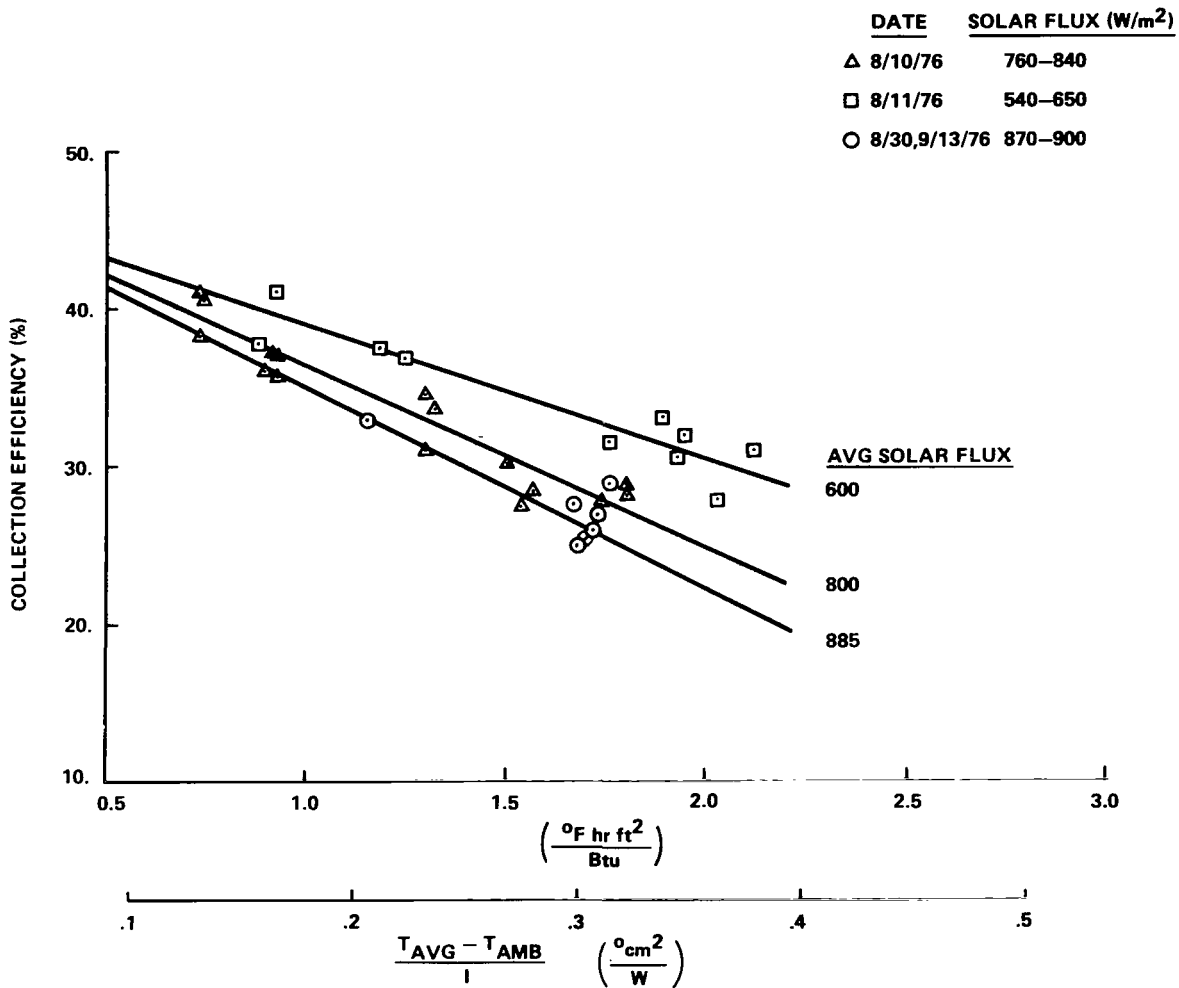
Figure 19. Effects of solar flux variations on measured collection
efficiency versus ΔT/I.

aperture data. When the same data were plotted in terms of efficiency versus
average fluid temperature (or tube inlet temperature), the scatter was reduced
to a reasonable level (Fig. 20). The influence of solar flux level is more
visible with the data arranged in terms of total energy loss versus average fluid
temperature at various solar flux levels. As represented by Figure 21, energy
lost is a function of fluid temperature and incident solar flux. However, at a

COLLECTION EFFICIENCY (%)

50

40

30

20

10

0   100   200   300   400   500   600

(°F)

TEST CONDITIONS

● SOLAR FLUX (W/m²)
□ 540 - 650
△ 760 - 840
○ 870 - 900
● FLOWRATE: 70-290 kg/hr

0   100   200   300

AVERAGE FLUID TEMPERATURE (°C)
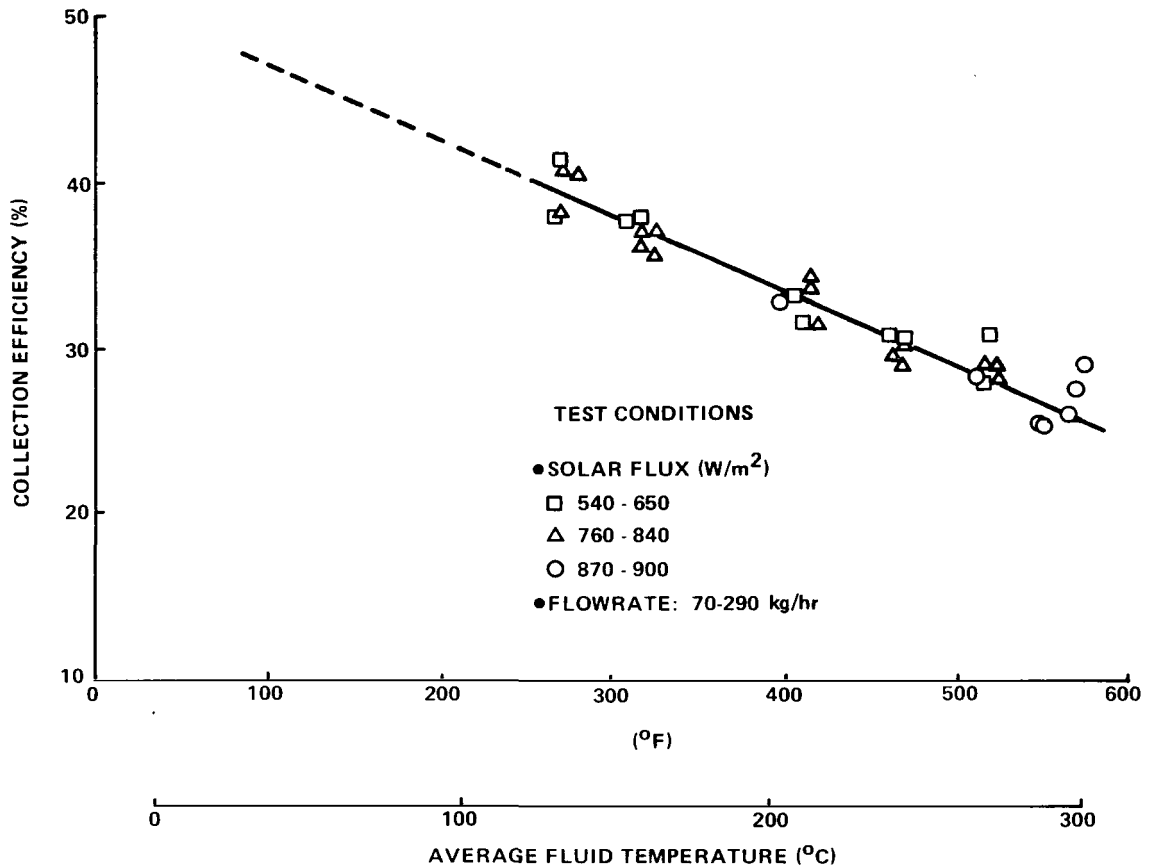
Figure 20. Measured collection efficiency versus fluid temperature.

given fluid temperature, the energy loss and, conversely, energy collected are directly proportional to the solar flux. Figure 22, derived from Figure 21, illustrates that efficiency did not vary with solar flux at a constant fluid temperature. Results with the focused aperture were similar although the efficiencies indicated a slight upward trend with increasing solar flux. Therefore, it can be concluded that fluid/tube temperature was the primary thermal parameter affecting collector efficiency with the present receiver configuration at solar flux levels from 470 to 900 W/m².

2. Flowrate. The influence of mass flowrate on collection efficiency was generally not discernible. The measured efficiency data in Figures 23 and 24 are arranged in terms of flowrate ranges and indicate no obvious efficiency trends with flowrate. It was noted that the data seemed to be more erratic at flowrates less than 70 kg/hour where the flowrate/temperature combination resulted in laminar turbulent transitional flow.
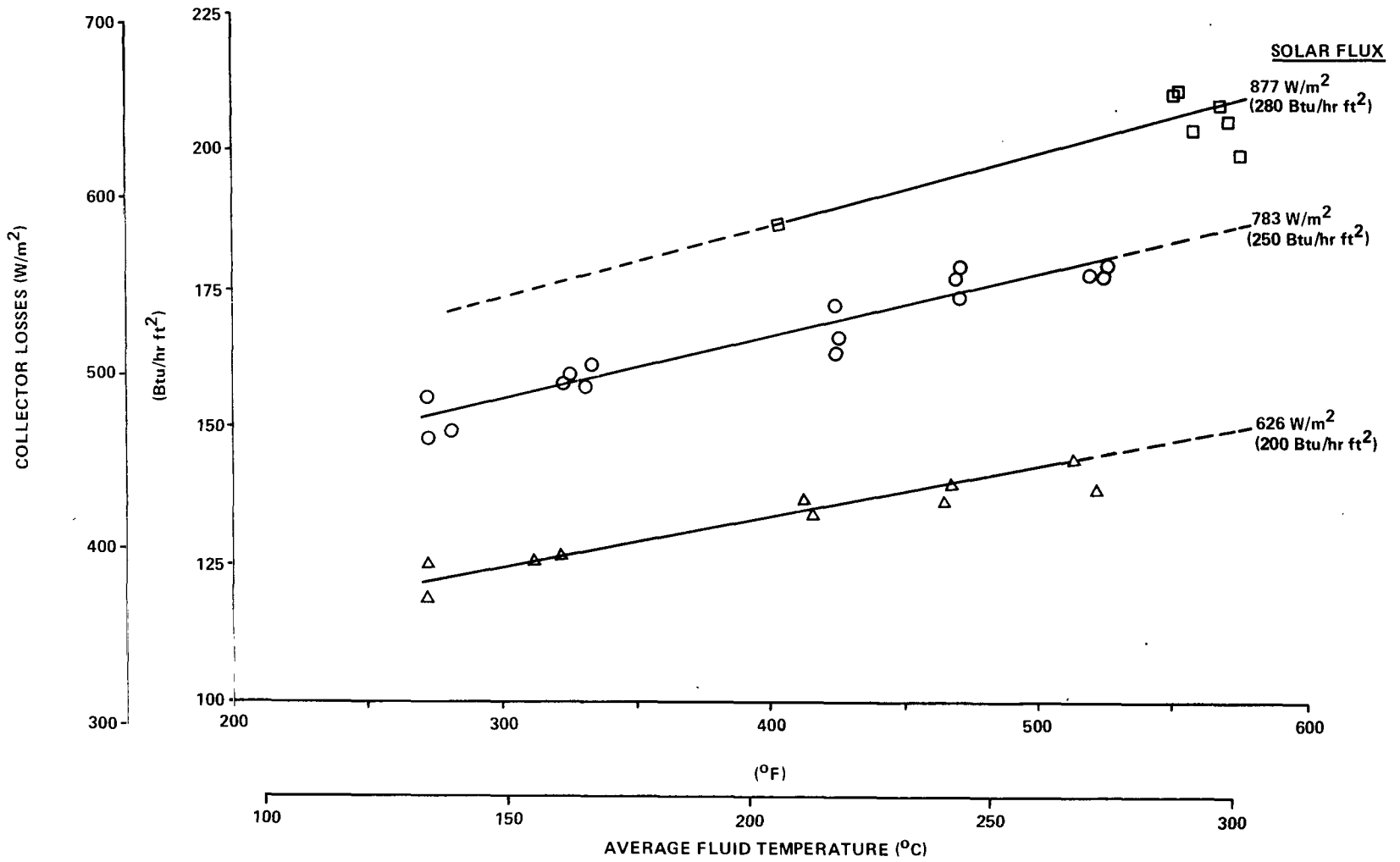
Figure 21. Collector losses versus fluid temperature at various solar flux levels.
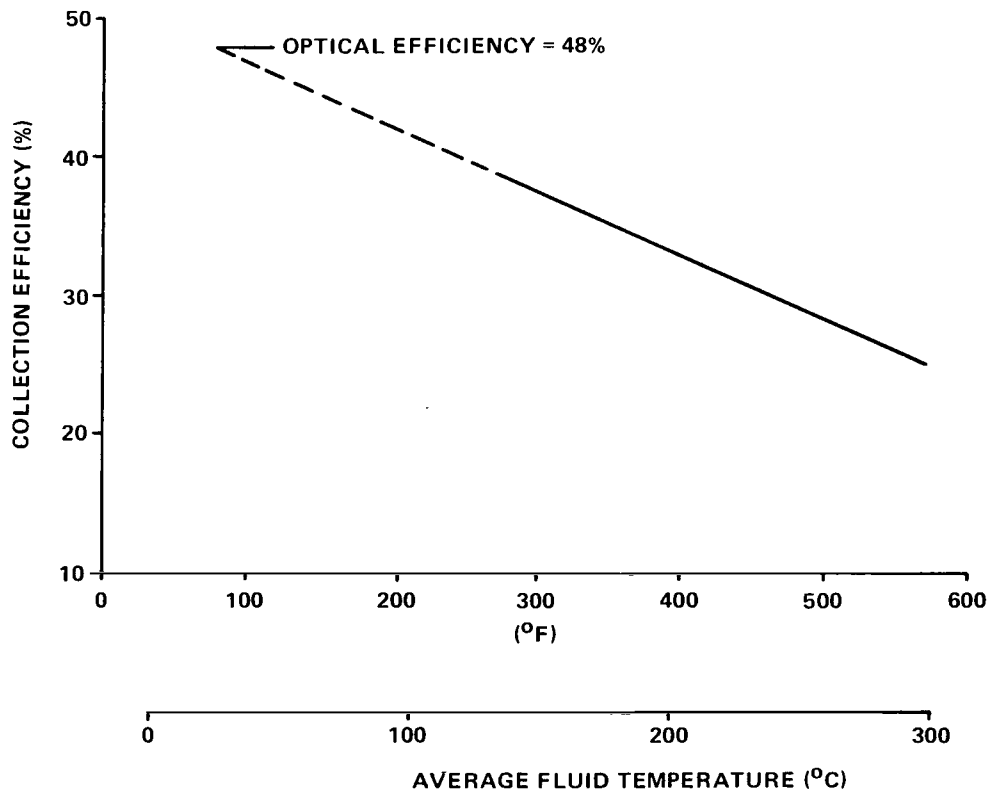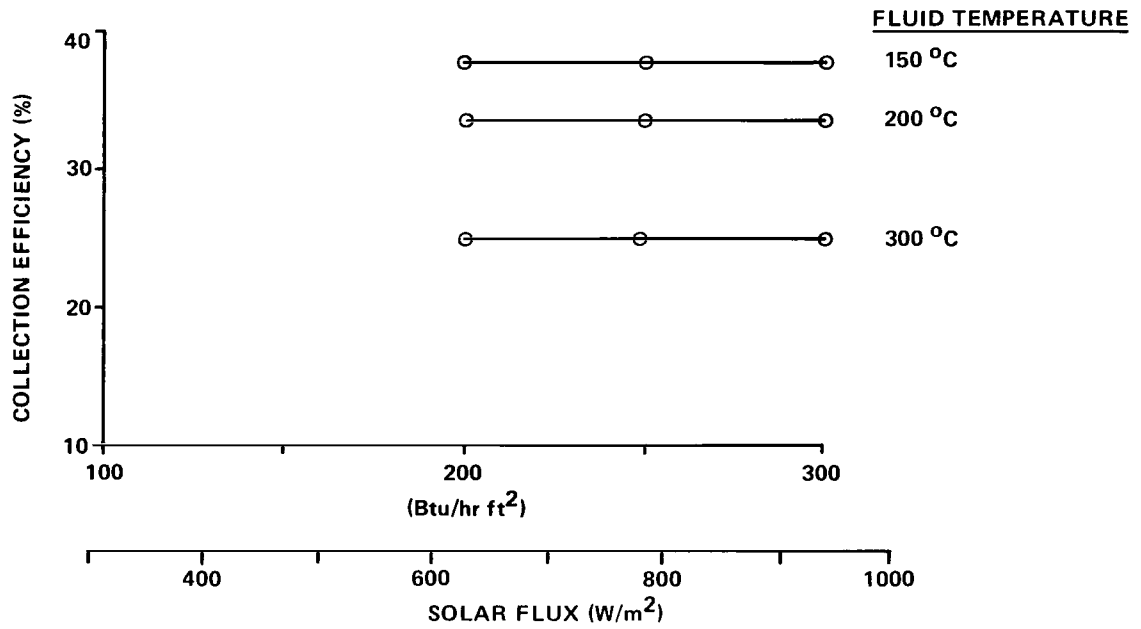
Figure 22. Solar flux and fluid temperature effects on collection efficiency.

COLLECTION EFFICIENCY (%)

CONDITIONS
• DEFOCUSED APERTURE
• FEP WINDOW
• FLOWRATE (kg/hr)
  △ 224 - 293
  ○ 150 - 200
  □ 120 - 126

(°F)

(°C)

COLLECTION EFFICIENCY (%)

CONDITIONS
• FOCUSED APERTURE
• FEP WINDOW
• FLOWRATE (kg/hr)
  △ 228 - 303
  ○ 154 - 156

(°F)

AVERAGE FLUID TEMPERATURE (°C)

Figure 23. Measured effects of aperture focusing/defocusing and
flowrate on collection efficiency (with FEP).

38

Figure 24. Measured effects of aperture focusing/defocusing and
on collection efficiency (without FEP).
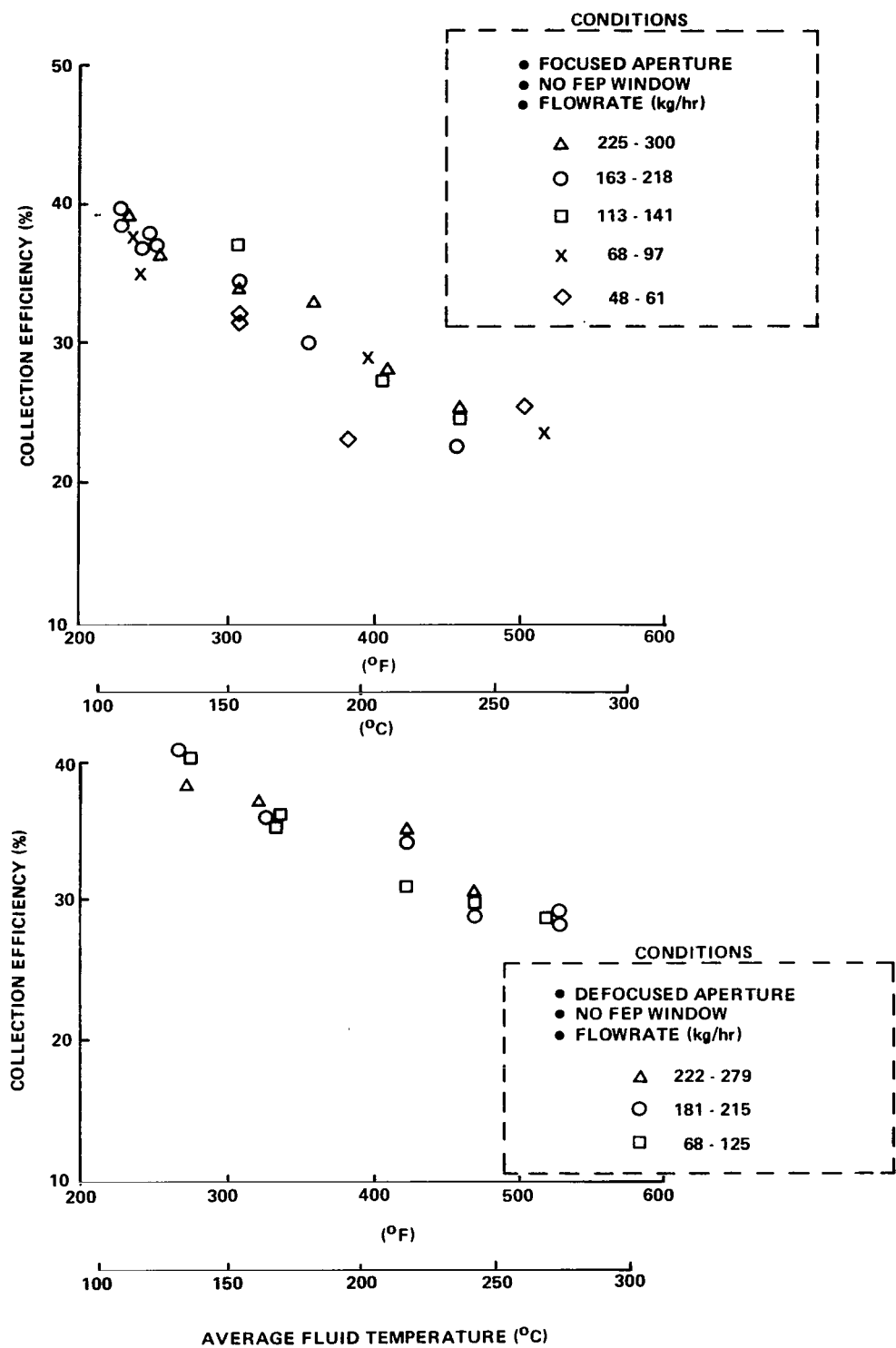
3. **FEP Window.** The FEP cover was not a dominant effect on collector performance. The measured performance with and without the FEP is represented by Figures 23 and 24. The maximum measured efficiencies at temperatures above approximately 230°C occurred with the FEP; whereas, at lower temperatures, the performance was not affected. It is surmised that the optical losses with the present receiver configurations overshadow the tube thermal losses; therefore, the benefits of a transparent cover should become more apparent with a modified receiver operating at higher efficiencies. No visible degradation of the FEP material occurred during the testing.

VII. RECEIVER ASSEMBLY THERMAL ASSESSMENT

Areas of interest at the component level included the ALZAK temperatures, absorber tube wall-to-fluid temperature differentials, and receiver assembly thermal loss characteristics. The receiver assembly measurement locations utilized are described in Figure 10. The ALZAK temperatures beneath the tube and the absorber tube circumferential temperature differentials were measured near the midpoint and exit of the receiver assembly.

A. ALZAK Temperatures

The ALZAK material has an upper temperature limit of 230°C per the manufacturer's recommendation. A concern was whether or not this upper temperature limit would be exceeded in localized areas. Since the absorber tube bottom surface is within 0.25 cm of the ALZAK surface, the selected measurement locations should represent maximum temperature positions. Measured ALZAK temperatu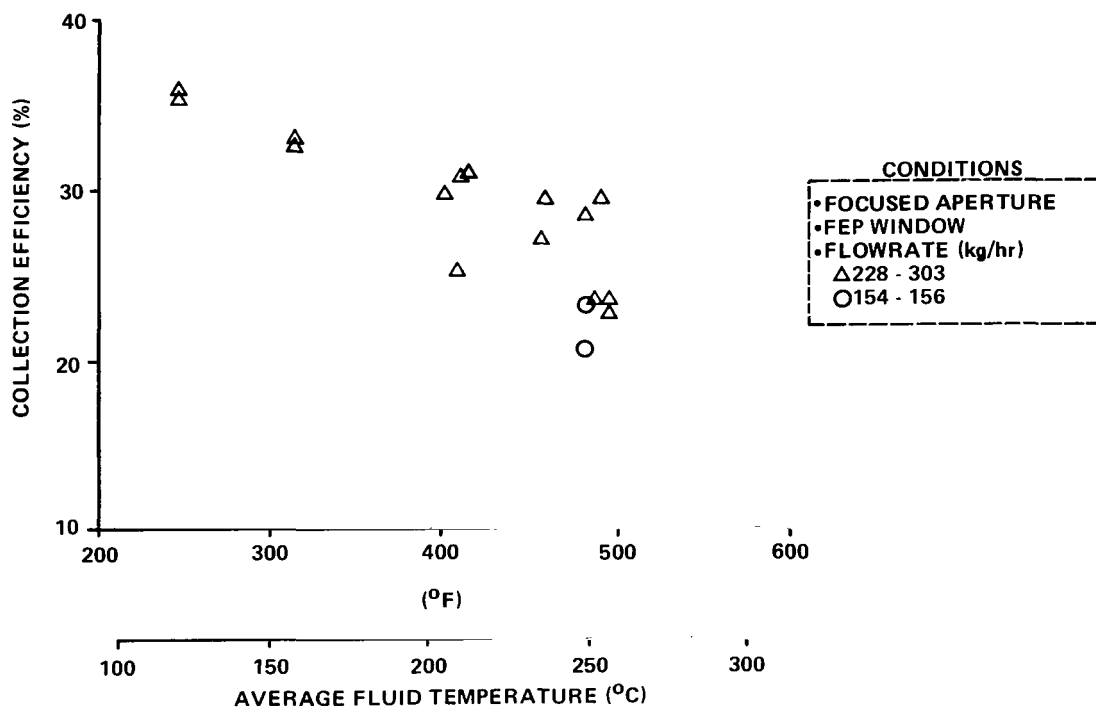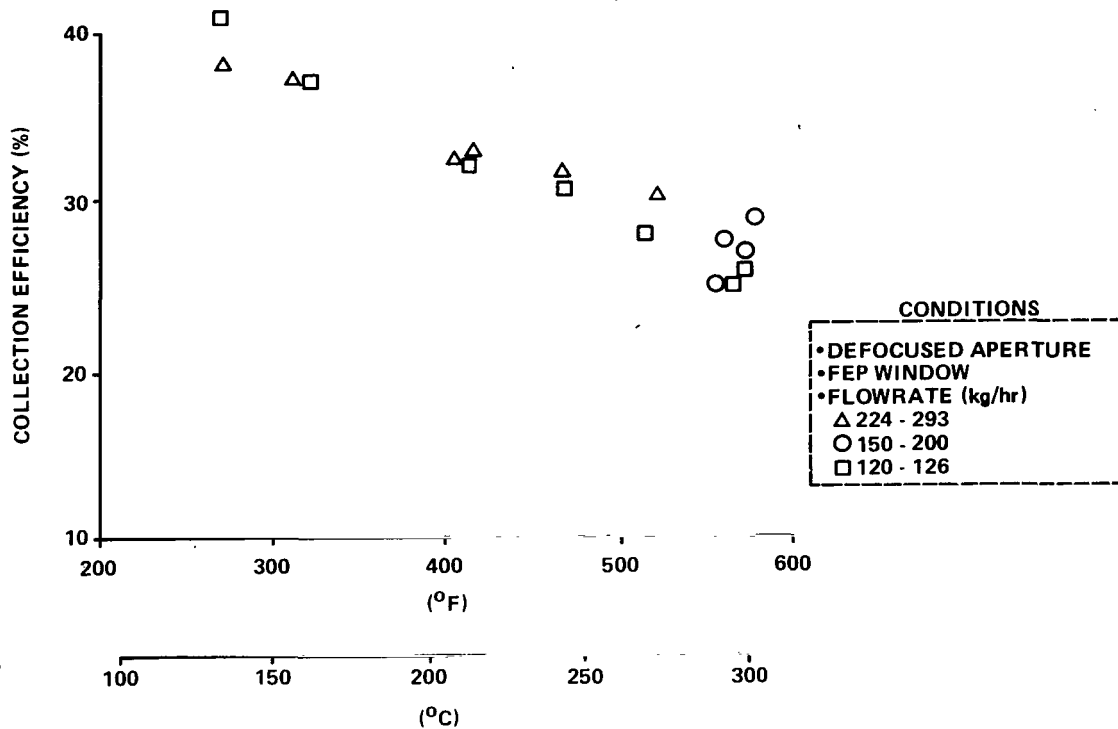res at the receiver assembly midpoint and outlet are presented in Figures 25 and 26, respectively. The FEP cover and absorber tube fluid temperature were major influences with maximum temperatures occurring at the tube outlet with the FEP cover. The maximum temperature measured was 220°C with a fluid temperature of 310°C. Therefore, the ALZAK temperature limit was approached but not exceeded. The FEP forced retention of heat within the reflective cavity and resulted in higher ALZAK temperatures. Removal of the FEP lessened the response of ALZAK temperature to tube fluid temperatures. The ALZAK temperatures increased with increasing solar flux, but the effect was secondary. Referring to Figure 26, with a fluid temperature of 260°C maximum temperatures were 180°C and 200°C with the aperture focused and defocused, respectively. Removal of the FEP lowered maximum temperatures to less than 150°C.
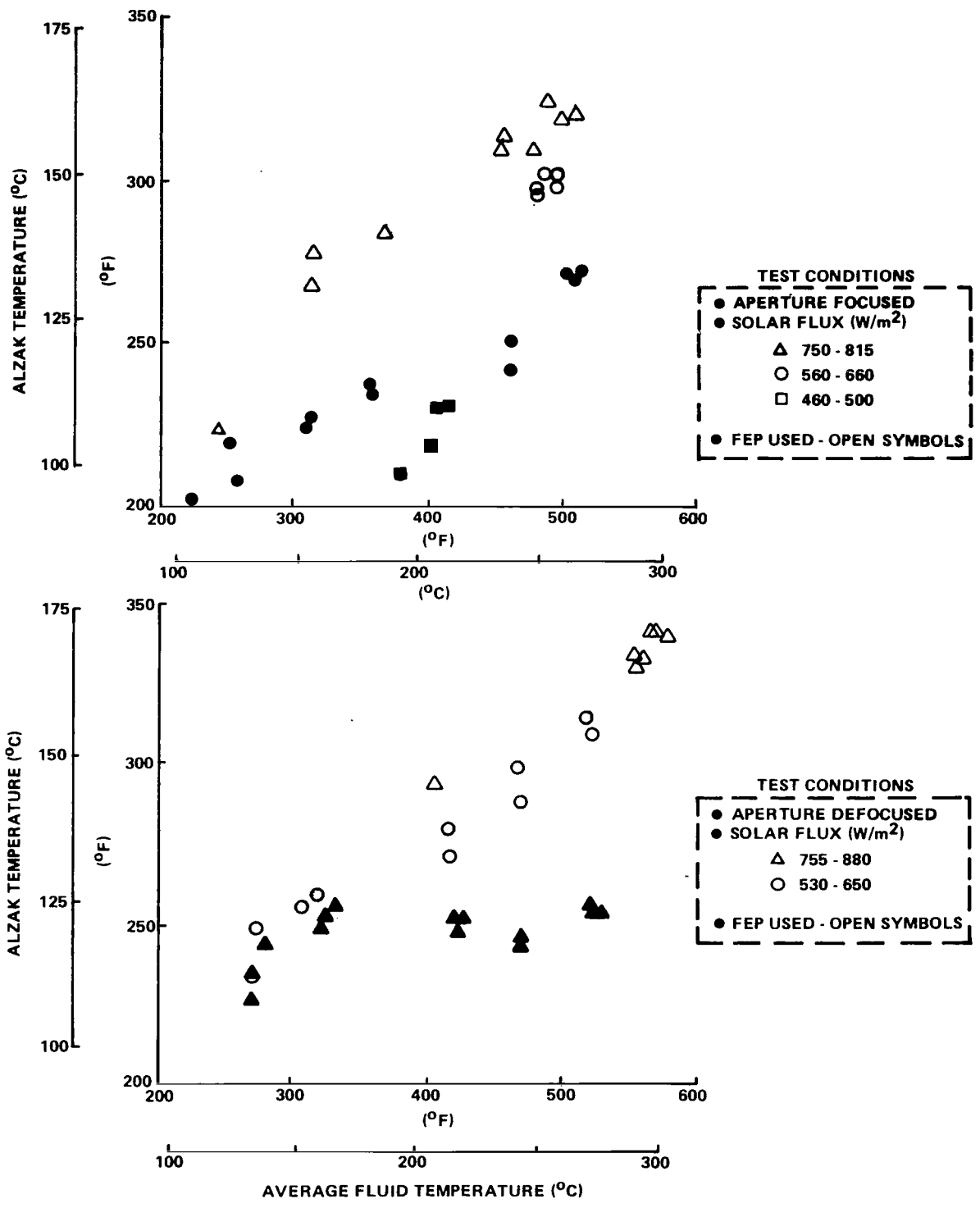
Figure 25. Measured ALZAK temperatures at the longitudinal midpoint.
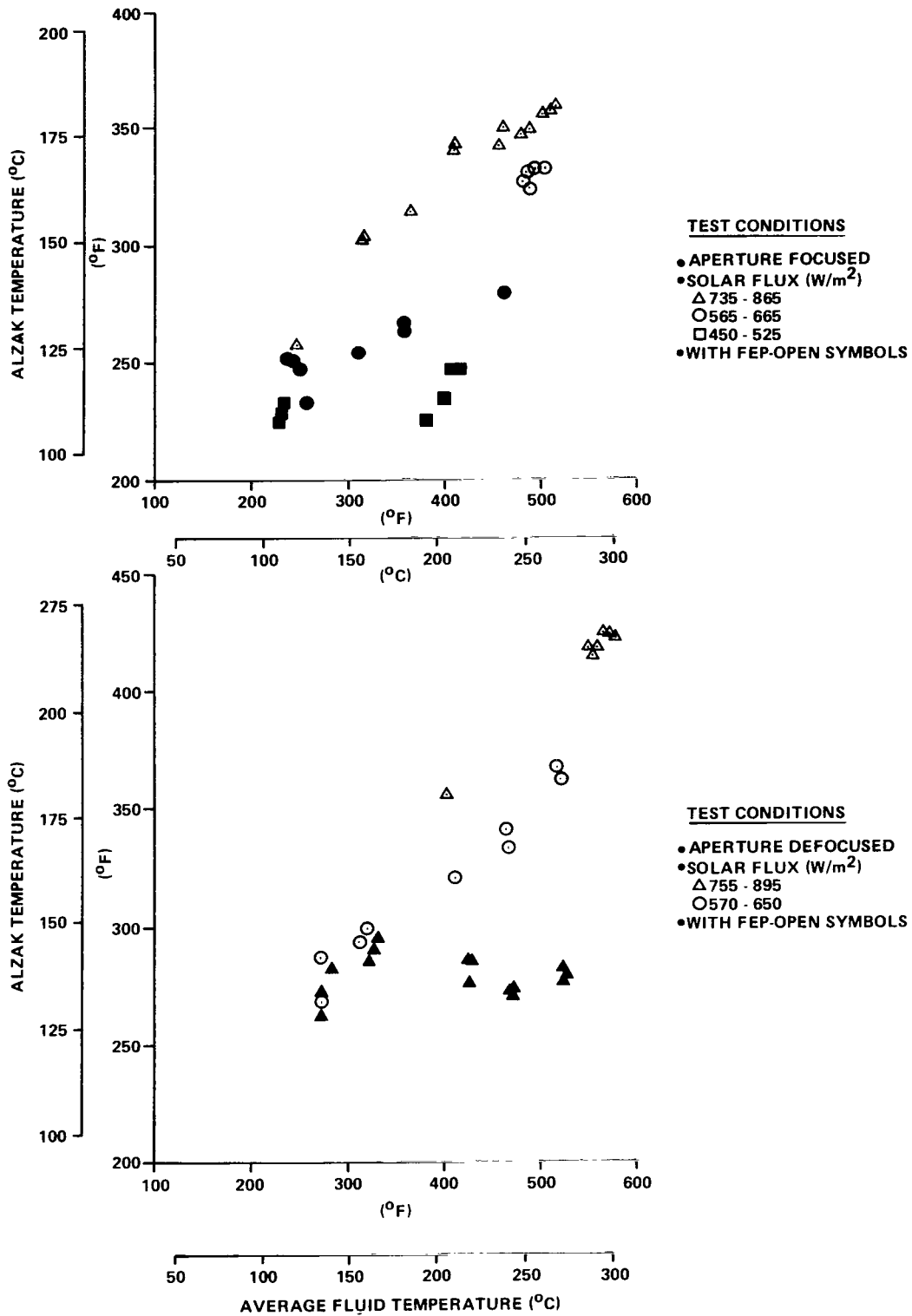
Figure 26. Measured ALZAK temperatures near the receiver outlet.

B. Absorber Tube Gradients

The energy is concentrated primarily on the upper half of the absorber tube. Therefore, a concern at the component performance level was localized heating effects, i.e., inefficient heat transfer to the transport fluid and excessive film temperatures (greater than 374°C) at the tube wall. The maximum measured tube wall-to-fluid and circumferential temperature differentials are presented in Figures 27, 28, and 29. Major test variables included fluid flowrate, fluid temperature, and incident solar flux. The temperature differentials were primarily controlled by fluid flowrate and temperature. For example, at 4.5 liters/min the tube-fluid and circumferential differentials were less than 20°C and 10°C, respectively, for the entire range of other test conditions. At the minimum flowrate/temperature combination of 2.3 liters/min and 120°C, the maximum tube-fluid and circumferential temperature differentials were 55°C and 22°C, respectively (Figs. 27 and 29); whereas, at fluid temperatures above 225°C, the tube-fluid and circumferential gradients were less than 20°C and 10°C, respectively.

A lower level effect was that of solar flux. The gradients increased with solar flux (compare Figs. 27 and 28), but the effects became secondary at fluid temperatures above 200°C. Gradients were also a function of longitudinal position on the tube. Since the fluid heating is initiated at the tube entrance, the tube-fluid temperature differentials were consistently higher at the entrance than at the exit. The tube wall gradients were also generally highest at the entrance; however, the inlet to outlet deviations were ordinarily insignificant. Additional factors considered that apparently did not significantly affect the temperature differentials included removal of the FEP aperture cover and aperture focusing/defocusing.

The fluid flowrate/temperature influence can be visualized in terms of Re number. The "smooth tube" Re number at 120°C is approximately 1200 and 2300 at 2.3 and 4.5 liters/min, respectively. Similarly, the Re number increased with fluid temperature to, for example, 6800 at 300°C/2.3 liters/min. The maximum measured tube-fluid temperature difference (at tube entrance) versus Re number is presented in Figure 30 for various volumetric flowrate and solar flux conditions. The temperature differentials increased rapidly below an Re number of approximately 2000. An example conclusion is that at an Re number of 1900, the bulk fluid operating temperature would be limited to 344°C or less to prevent exceeding the film temperature limit of 374°C.
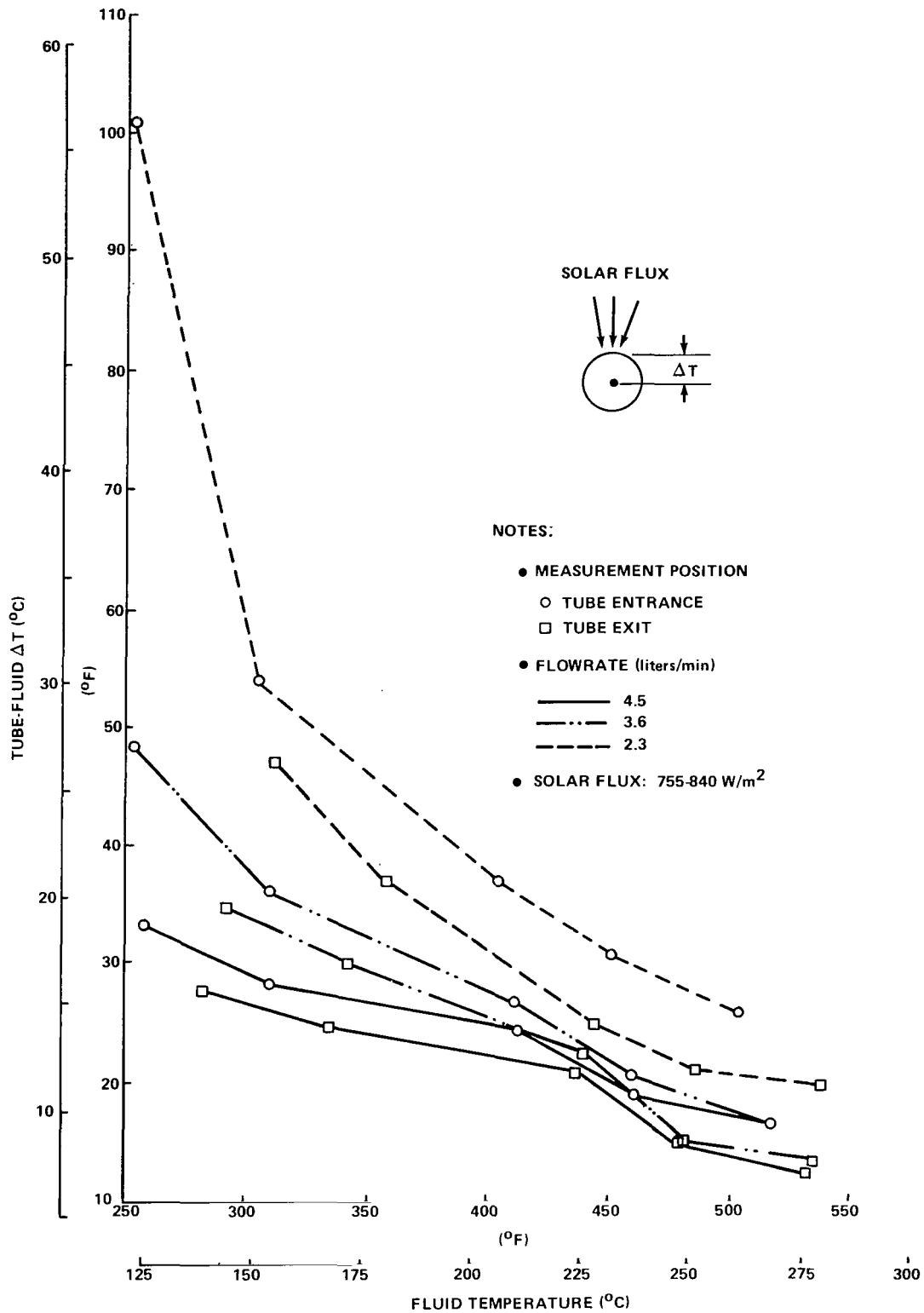
Figure 27. Measured absorber tube wall-to-fluid temperature differentials.
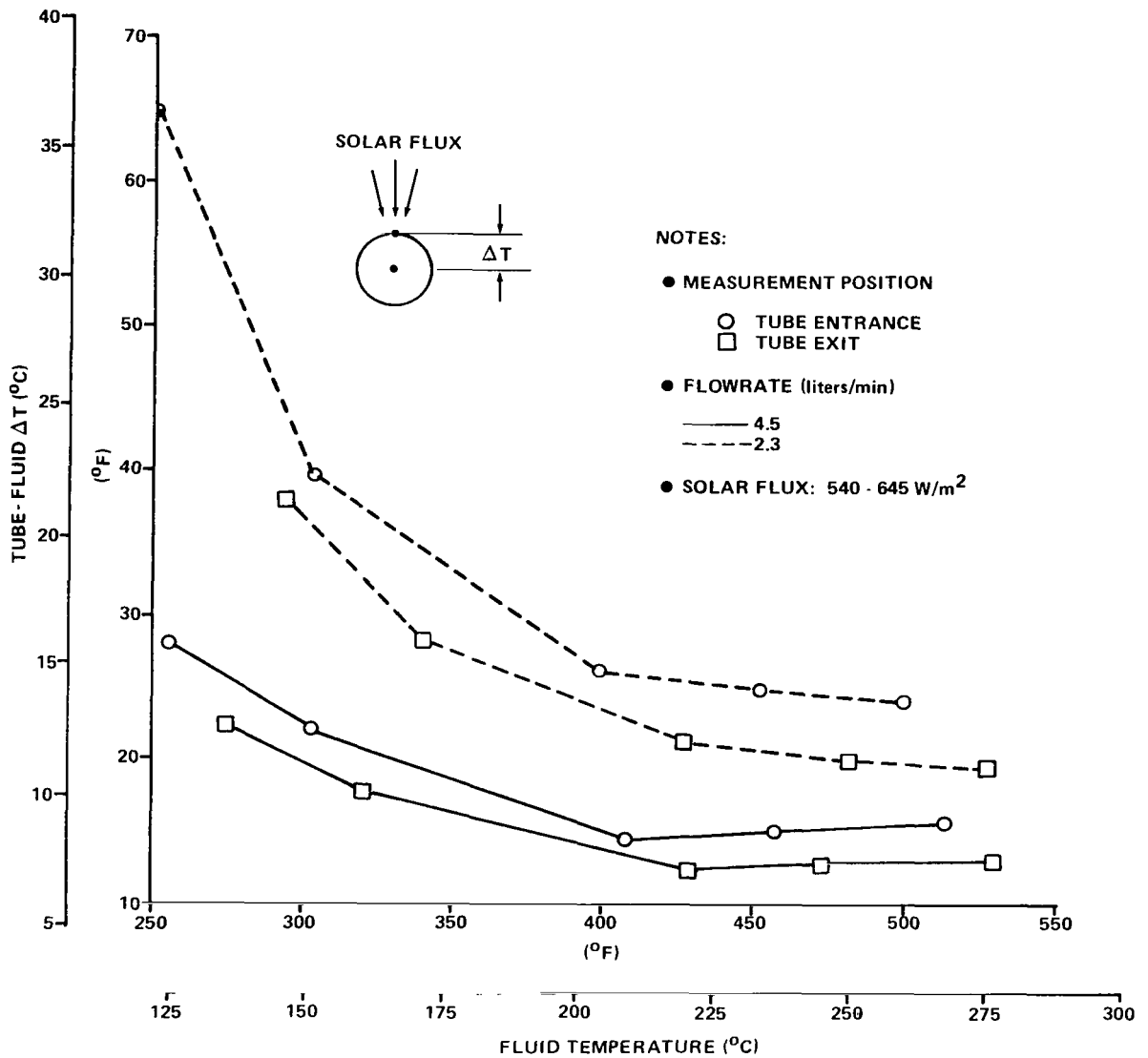
Figure 28. Measured absorber tube wall-to-fluid
temperature differentials.

It is estimated that the corrugated tube Re number for a given set of conditions is approximately twice that of a smooth tube. Therefore, at $R_e \leq$ 2000, the flow apparently was in the turbulent to laminar transition regime. Re number was the dominant influence, but at a given Re number the temperature difference increased with increasing solar flux and, to a lesser degree, with decreasing flowrate.

45
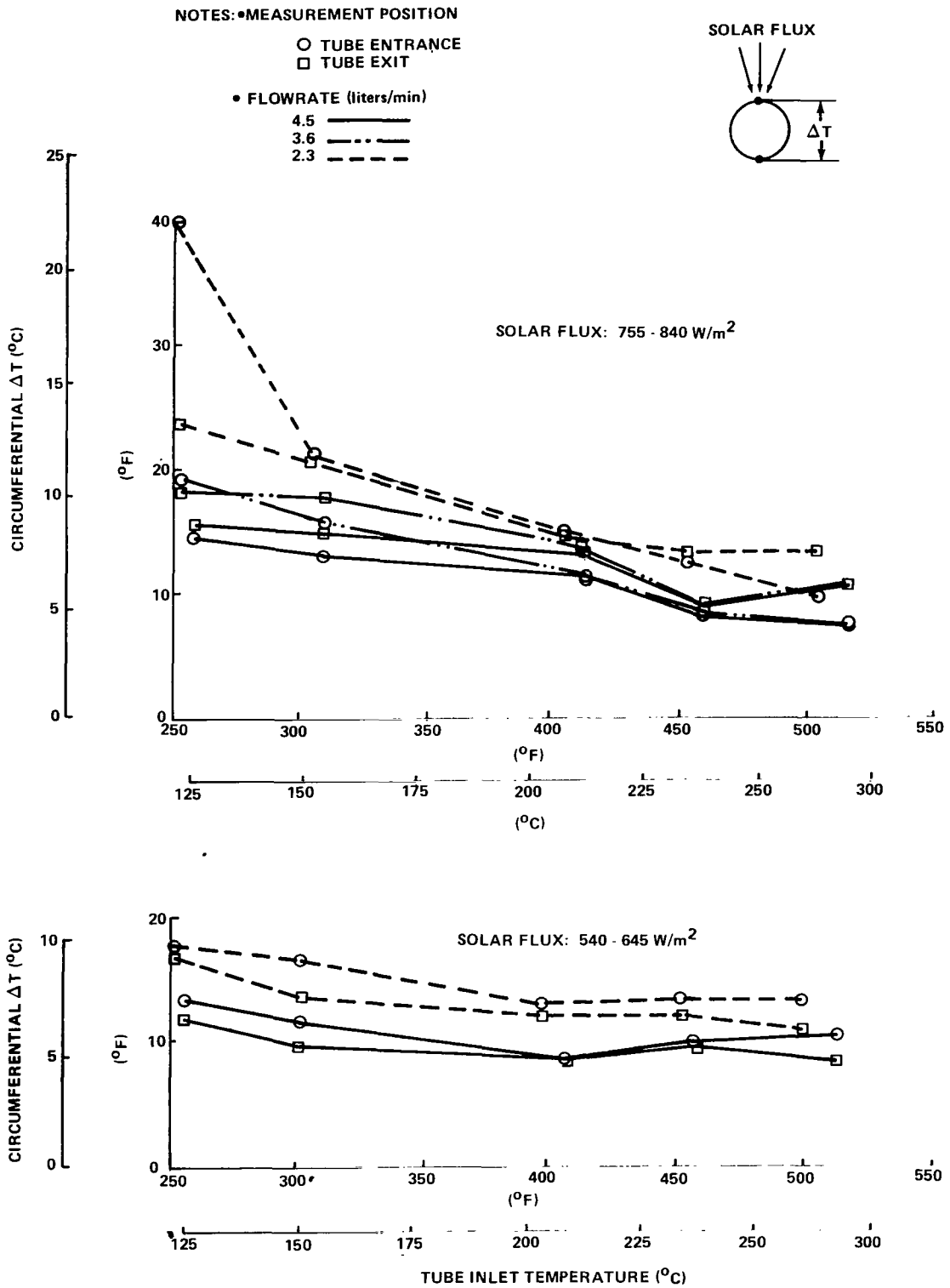
Figure 29. Measured absorber tube circumferential temperature differentials.

46
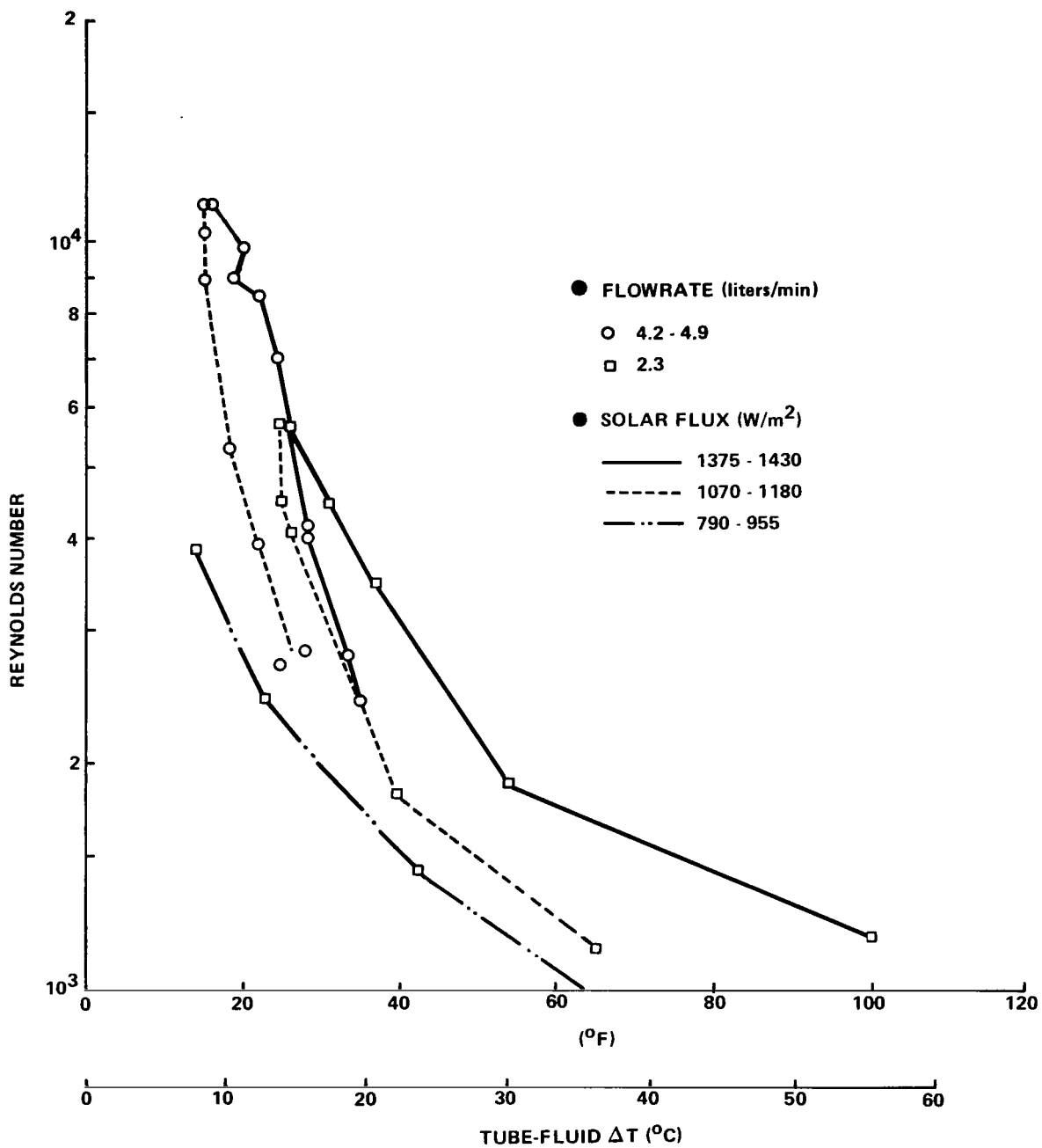
Figure 30. Measured absorber tube wall-to-fluid temperature differentials versus Reynolds number.

C. Receiver Thermal Performance

The thermal performance characteristics of the receiver assembly were assessed assuming a defocused receiver. Based on the measured lens and collector performance data, the receiver collection efficiency versus fluid temperature was estimated and is presented in Figure 31. The receiver averaged efficiency varied linearly from 50 percent at 120°C to 32 percent at 300°C. The receiver overall loss coefficient of heat transfer decreases with increasing fluid temperature and increases with increasing solar flux (Fig. 32). At a solar flux of 880 W/m^2, the loss coefficient was 9.3 and 5.0 W/m^2 at 130°C and 270°C, respectively. The corresponding range with a solar flux of 600 W/m^2 was 6.9 to 3.5 W/m^2°C. The coefficient trend with solar flux is consistent with the previous conclusion that collection efficiency is independent of solar flux within the range tested. Therefore, at a given temperature, the loss coefficient increases with solar flux to compensate for the constant receiver efficiency.
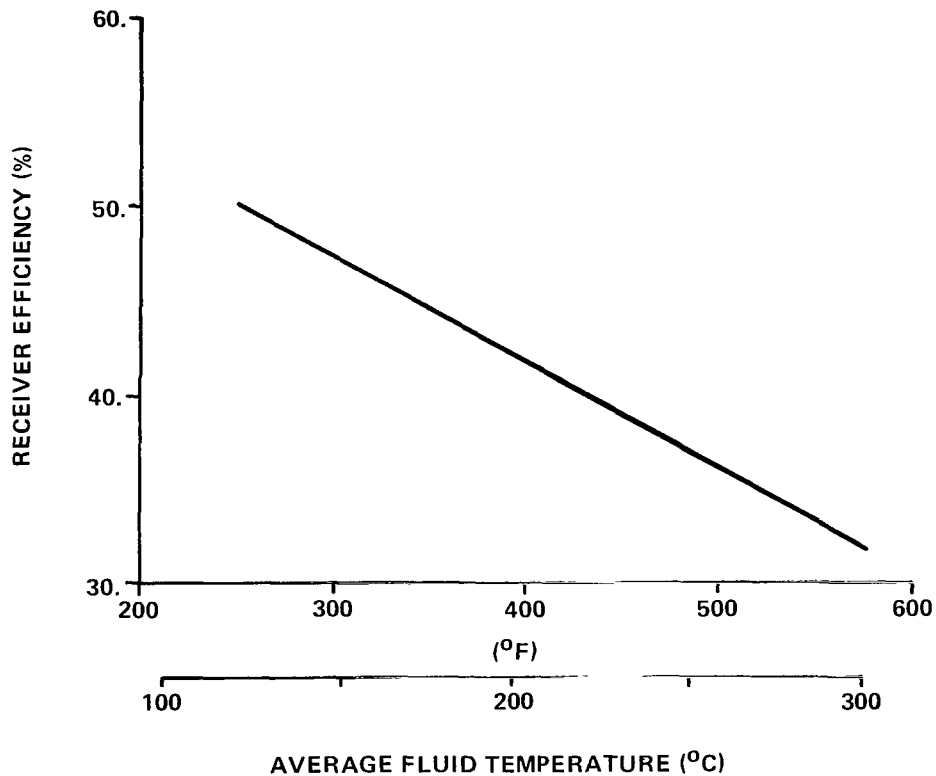
Figure 31. Defocused receiver assembly collection efficiency variation.

48
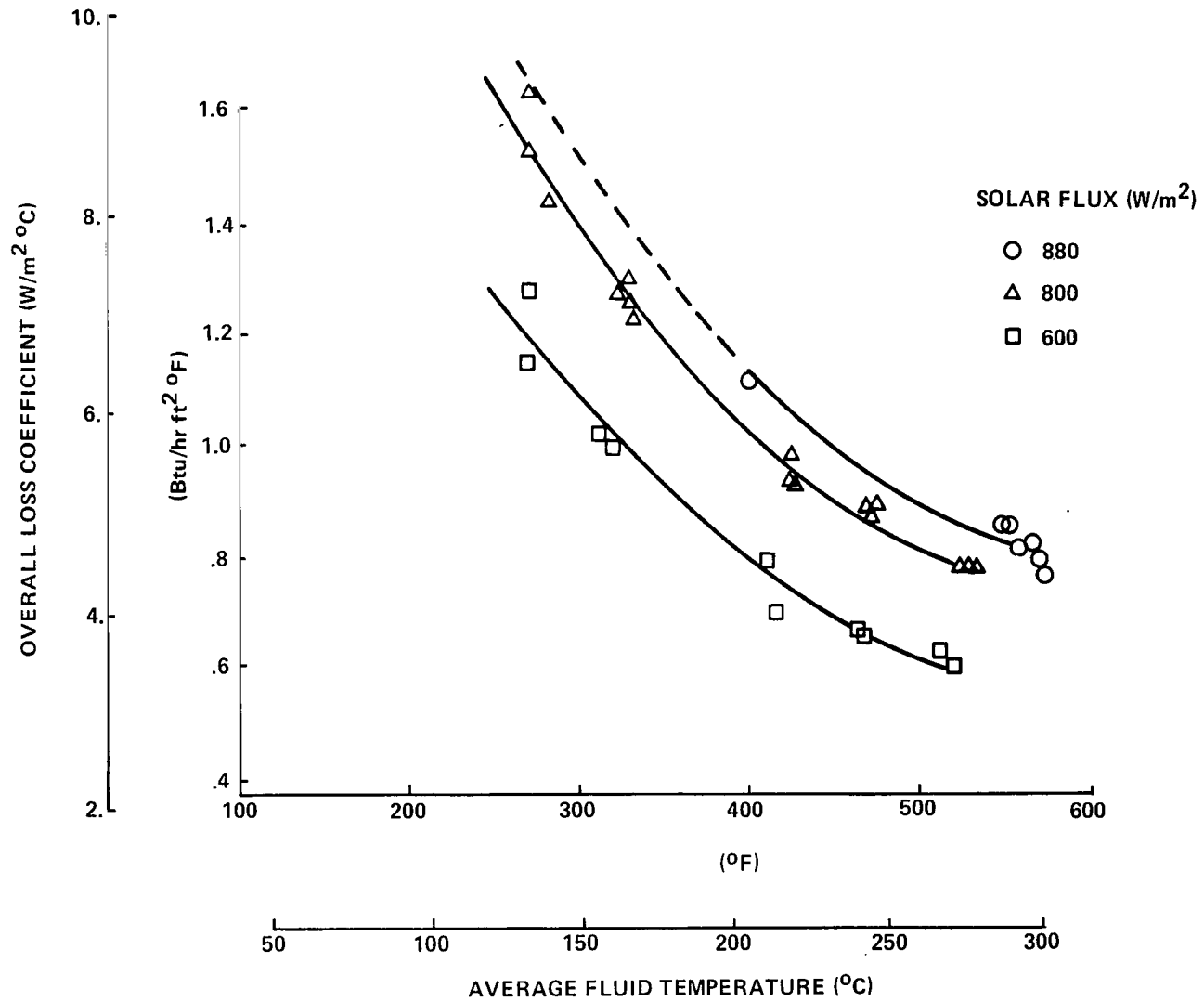
Figure 32. Receiver assembly overall loss coefficient variation.

A measure of energy losses from the absorber tube was obtained by observing the fluid inlet-to-outlet temperature decreases with no solar flux imposed. Figure 33 presents the measured thermal loss and equivalent heat transfer loss coefficient versus average fluid temperature with and without the FEP aperture cover. Due to the small temperature decreases measured (approximately 1° to 4.5°C), the data accuracy degraded somewhat and resulted in some data scatter. The thermal loss ranged from approximately 170 to 420 W over a temperature range of 215° to 330°C with the FEP. The losses without FEP averaged 10 percent higher. The loss coefficients averaged 9.4 and 10.4 $W/m^2 \cdot C$ (1.68 to 1.85 Btu/hr-ft^2-° F) with and without the FEP, respectively.

The receiver assembly thermal loss characteristics were further assessed using auxiliary equipment to measure the external surface temperatures of the receiver assembly. As illustrated in Figure 34, the surface temperatures were measured at four locations, and the air temperature was measured at positions near the receiver, near the lens, and about midway between the lens and receiver. The surface temperatures increased with increasing absorber tube temperature and were higher with than without the FEP. The measured air temperatures did not vary significantly (Fig. 34). Air temperatures in the vicinity of the receiver and lens averaged 47°C (117°F) and 44°C (112°F), respectively. Utilizing the measured temperatures on/near the receiver and assuming a loss coefficient of 11.2 W/m^2 °C (2 Btu/hour-ft^2-°F), external surface thermal losses versus tube inlet temperatures were estimated and are presented in Figure 35. It should be noted that losses through the reflective cavity aperture are not included. The thermal loss ranged from 175 W at 120°C to 380 W at 260°C without the FEP. With the FEP, the corresponding losses were 265 to 730 W. Therefore, the data illustrate that utilization of the FEP decreased reflective cavity convective losses but increased conductive losses. Thus, the net effect of the FEP was a small reduction in total losses.

VIII. COLLECTOR PERFORMANCE LOSS SUMMARY

The collector performance losses, optical and thermal, are summarized by Figure 36. Utilizing the measured collector efficiencies and a constant solar flux of 626 W/m^2, the total performance loss versus fluid temperature was computed for the defocused receiver position. The losses ranged from 2600 W at 130°C to 3200 W at 300°C. The constituent losses (based on component data) due to lens transmission, ALZAK reflectivity, tube absorptivity, receiver interception efficiency, and absorber tube thermal losses are also presented to illustrate relative magnitudes. The optical losses are constant and comprise 71 percent of the total losses. The lens transmittance and ALZAK reflectance
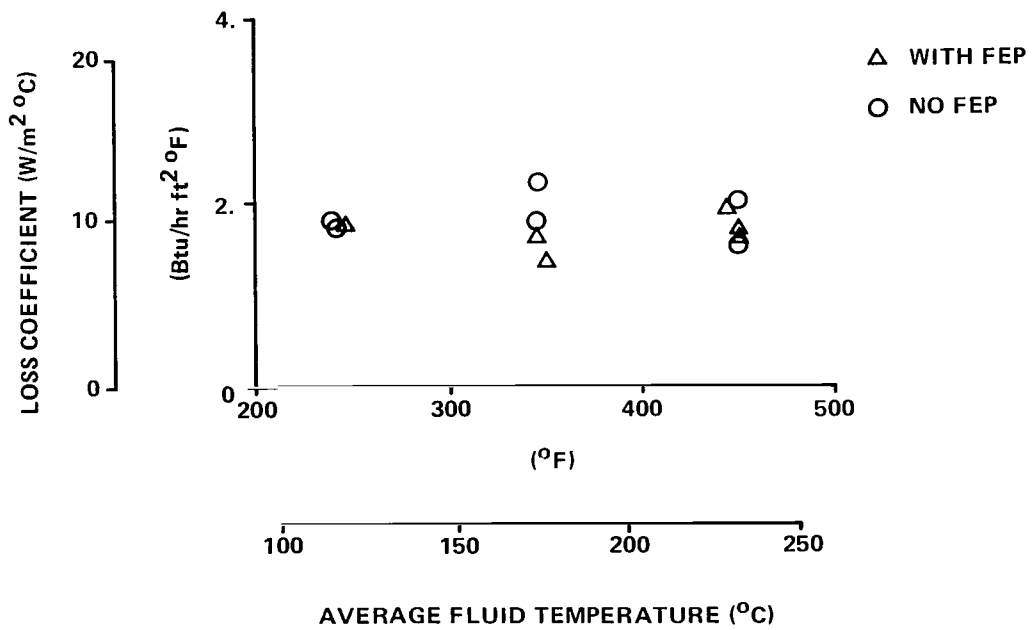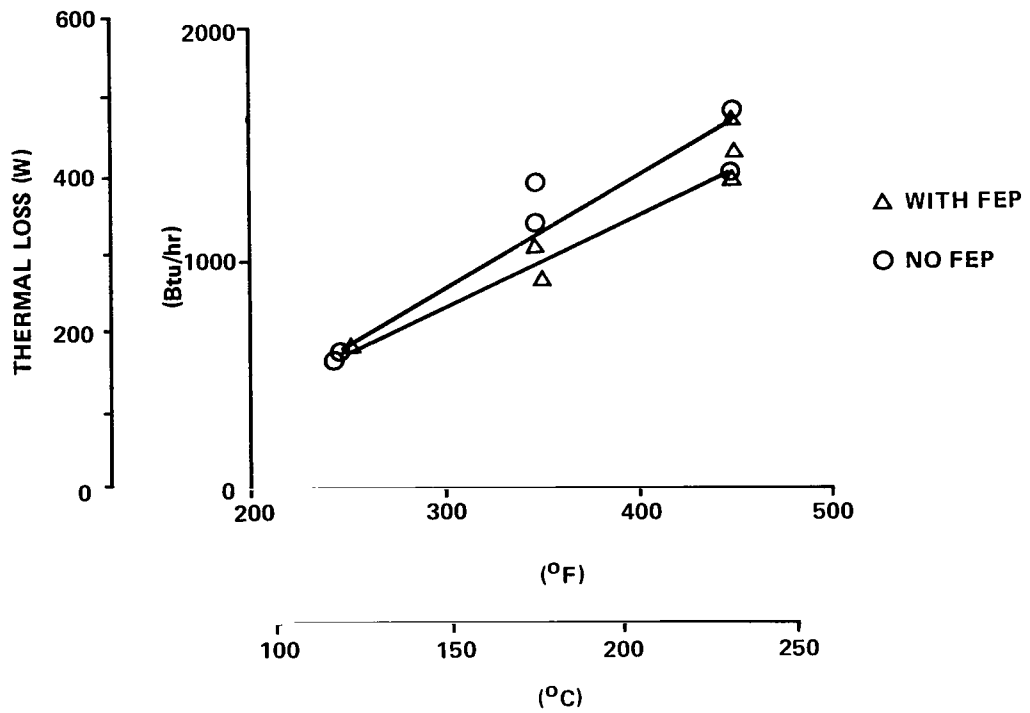
Figure 33. Experimental absorber tube thermal loss.
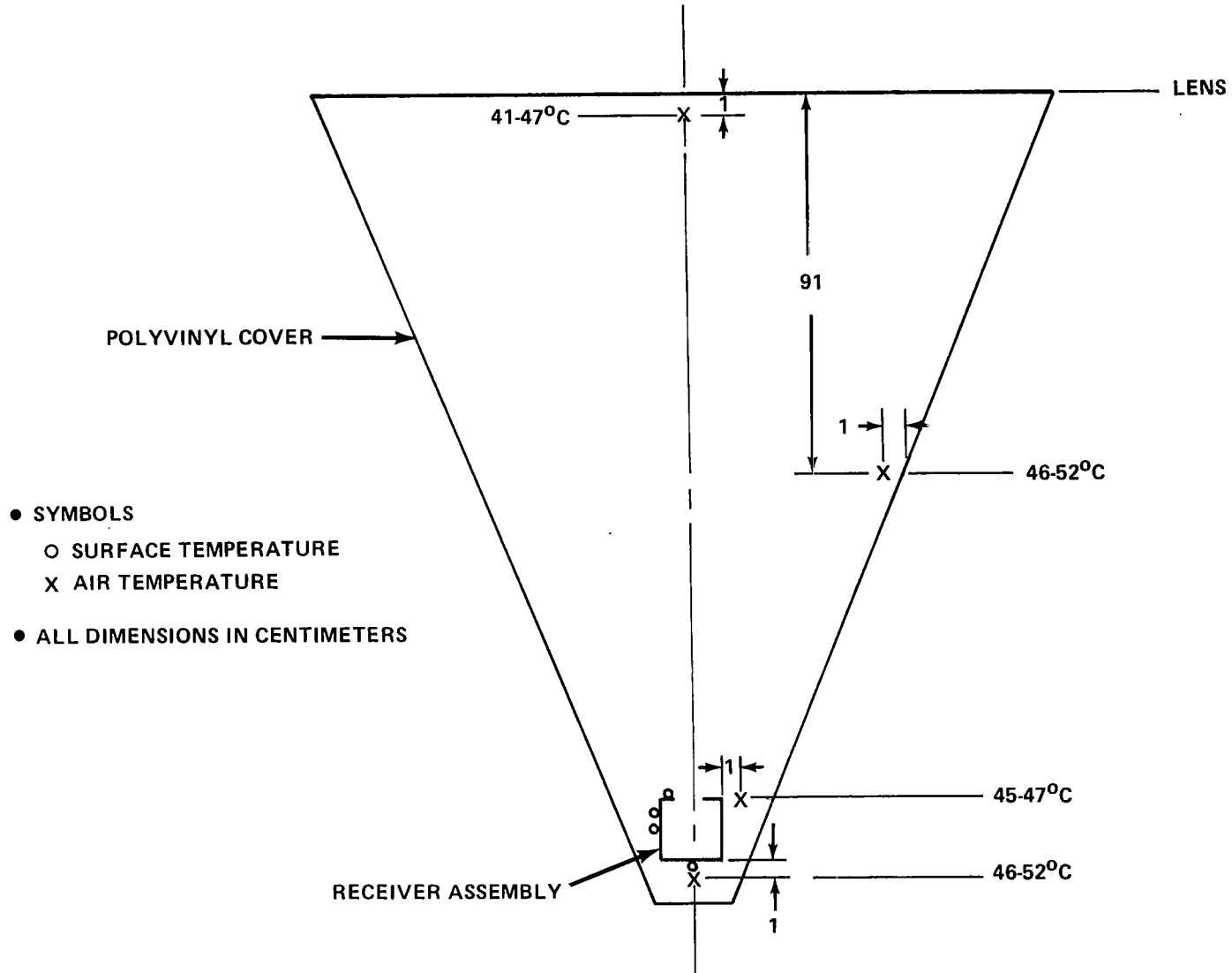
Figure 34. Auxiliary temperature measurements within collector
enclosure and on receiver external surface.
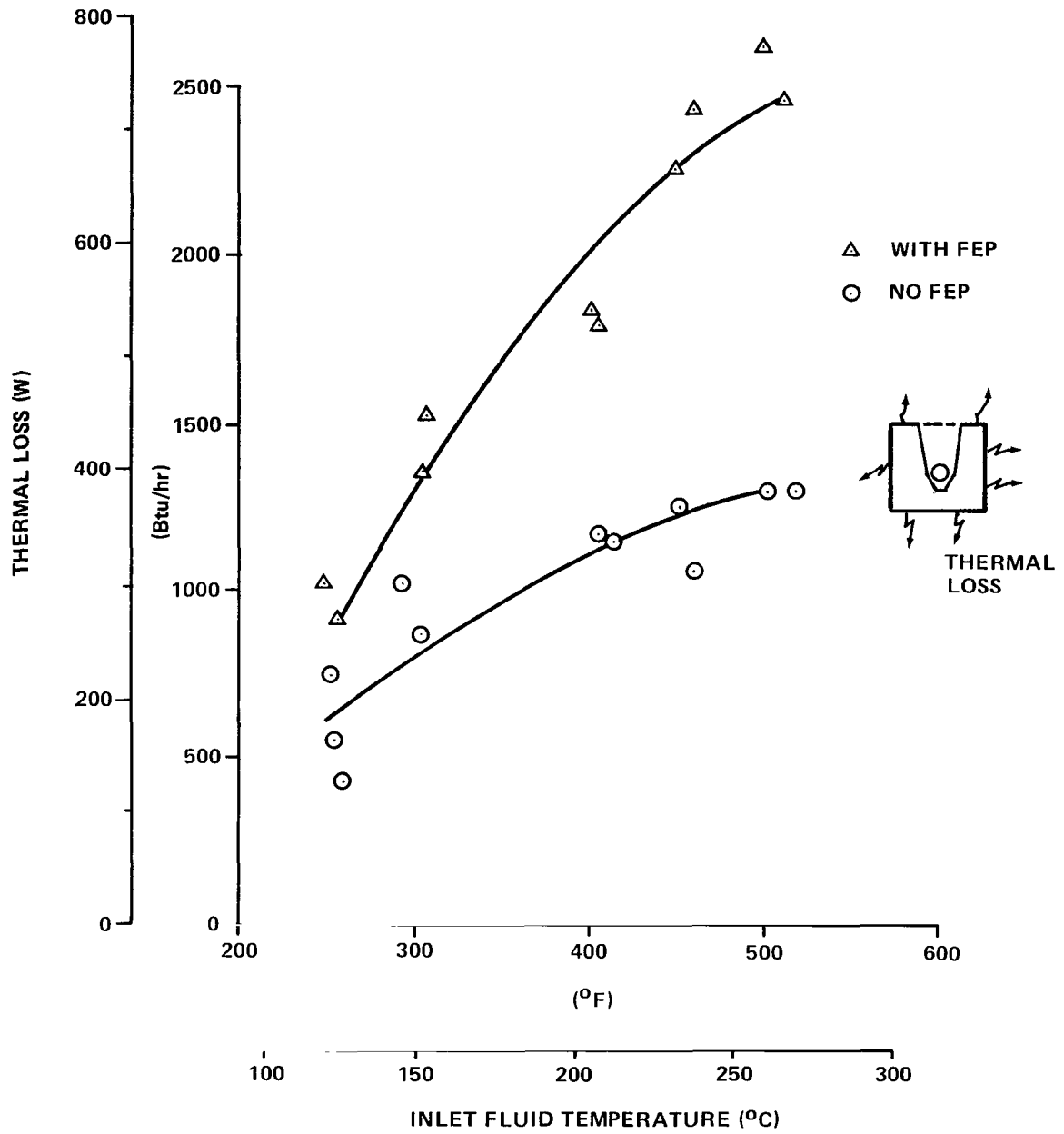
Figure 35. Receiver assembly thermal losses from external surfaces.
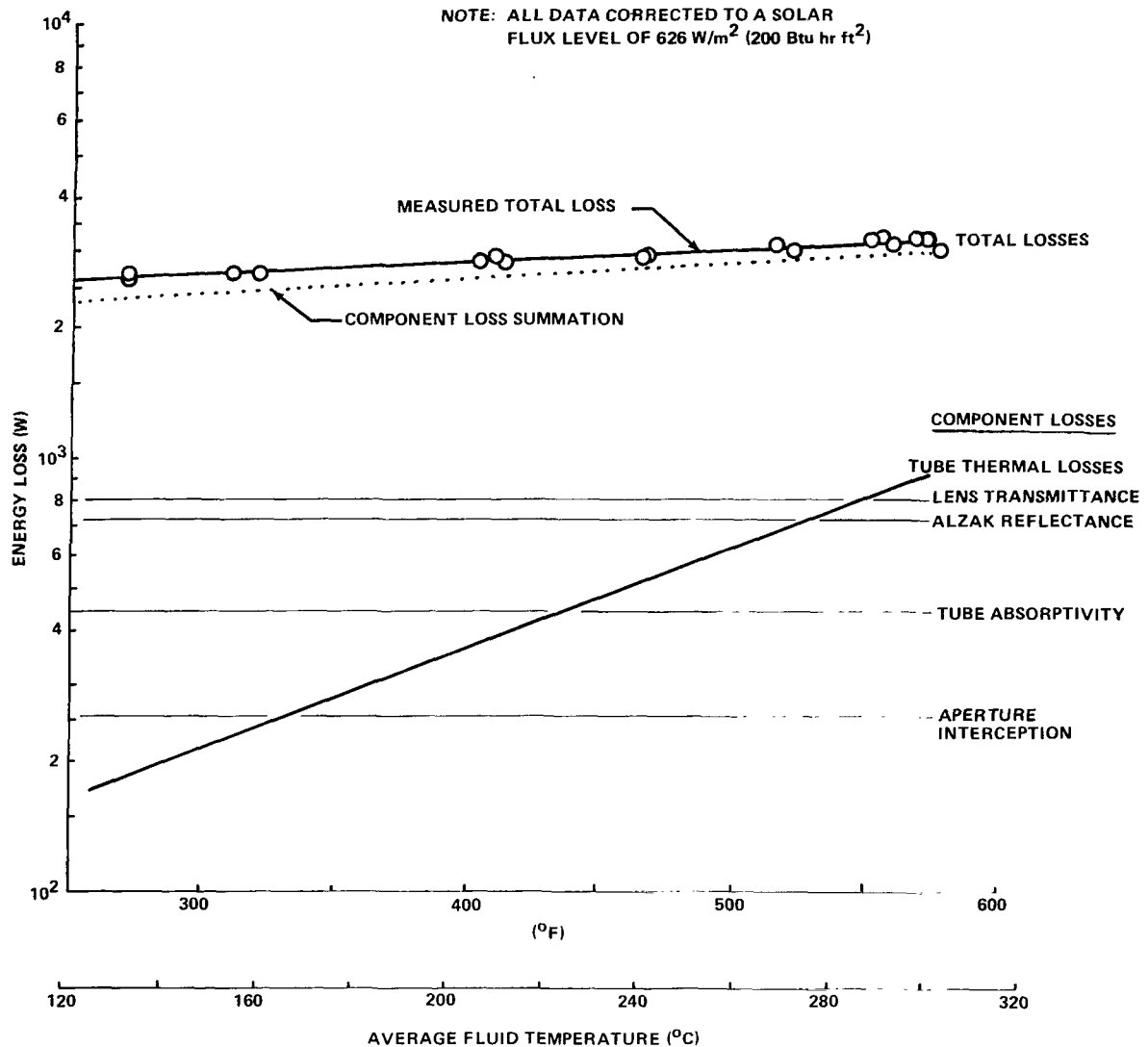
Figure 36. Collector performance loss summary.

are the primary optical losses and constitute 48 percent of the total. The tube thermal loss represents energy lost after it is absorbed (radiation and convection) and, hence, increases with temperature. The tube thermal loss represents 8 percent and 29 percent of the total at 150°C and 300°C, respectively.

The tube thermal losses cannot be significantly reduced without an evacuated environment. The lens transmittance can be improved, but not substantially. However, as discussed previously, by decreasing reliance on a reflective receiver cavity and increasing tube absorptance (Fig. 17), it appears that the performance losses can be significantly reduced.

IX. CONCLUSIONS

A. Lens Performance

1. Relative to the profiles produced by an earlier 56 cm lens, the focusing properties of the present 1.8 m lens were much improved. A baseline peak concentration of 61 and a 90 percent target width of 4.5 cm were computed for the 1.8 m lens. Bench testing indicated a peak concentration of 67 with a 90 percent target width of 4.2 cm. When assembled in the full scale configuration of 1.8 by 3.6 m, the nominal peak concentration and target width were 62 and 5 cm, respectively.

2. The primary effect of small transverse (E-W) Sun tracking deviations (< 1°) was the lateral shifting of the concentration profile. The target width increased linearly with tracking deviation. Example measured and analytical target width increases were 70 and 80 percent, respectively, to accommodate a ±0.5° deviation.

3. Lens performance was relatively insensitive to Sun-lens alignment in the longitudinal direction. Deviations up to 5° had no significant effects on peak concentration or profile width.

4. The measured and computed lens transmittance was 81 percent and 86 percent, respectively. Minor transmittance difficulties experienced with one of the two lens panel configurations should be correctable and enable a transmittance improvement to the 85 percent level in future lenses. Lens transmittance was not affected by Sun-lens misalignment within the range tested.

B. Collector Performance

1. With the receiver assembly aperture placed at the focal plane, the collection efficiency ranged from 40 percent at 90°C to 21 percent at 300°C. An efficiency of approximately 40 percent at 300°C had been predicted. The reflective cavity surrounding the absorber tube apparently did not reflect the concentrated solar flux to the tube as well as expected. This conclusion was verified by testing with the receiver cavity aperture defocused -2 percent, thereby increasing the energy directly focused on the tube. An efficiency increase to 26 percent at 300°C resulted.

2. Future receiver assemblies will involve placement of the absorber tube at the focal plane, thereby further increasing the energy directly concentrated on the tube. Reflective surfaces, if used, will serve in a backup rather than primary mode. Efficiency improvement to the 40 to 50 percent range at 300°C is anticipated.

3. Transverse Sun alignment deviations up to 0.5° had no measurable effect on collection efficiency. Longitudinal misalignments up to approximately 5° have no influence on efficiency, provided sufficient receiver length is available to accommodate the profile shifting along the tube.

4. Collection efficiency was essentially independent of solar flux magnitude within the 470 to 900 W/m^2 range.

5. The transport fluid (Therminol 66) flowrate had no discernible effect on efficiency in the 70 to 300 kg/hour range.

6. The FEP window removal degraded the efficiencies only slightly at fluid temperatures above 230°C. No FEP material degradation occurred.

7. Absorber tube temperature gradients were primarily controlled by fluid flowrate and temperature. At 4.5 liters/min the tube-to-fluid and circumferential temperature differentials were less than 20°C and 10°C, respectively. Maximum tube-to-fluid and circumferential gradients of 55°C and 22°C, respectively, occurred at a flowrate/temperature combination of 2.3 liters/min and 120°C.

8. An evaluation of total collector performance losses indicated that optical losses comprise 71 percent of the total. The lens transmittance and receiver cavity reflectance represented 48 percent of the optical losses. Tube thermal losses were 8 percent and 29 percent of the total at 150°C and 300°C, respectively. Decreasing reliance on a reflective receiver cavity and increasing the absorber tube diameter/absorptance should enable a 20 to 30 percent reduction in total losses.

REFERENCES

1. Cosby, R.: Performance, Manufacture, and Protection of Large Cylindrical Fresnel Lenses for Solar Collection. Final Report, Ball State University-Marshall Space Flight Center Cooperative Agreement, NCA8-00103, Modification No. 2, June 1975.

2. Rainhart, L. G. and Schimmel, W. P., Jr.: Effect of Outdoor Aging on Acrylic Sheet. SAND 74-0241, AEC Contract AT (29-1)-789, Sandia Laboratories Energy Report, Albuquerque, New Mexico, September 1974.

3. Cosby, R.: The Cylindrical Fresnel Lens as a Solar Concentrator. Final Report, Ball State University-Marshall Space Flight Center Cooperative Agreement, NCA8-00103, Modification No. 1, June 1975.

4. Hastings, L.; Alums, S.; and Cosby, R.: An Analytical and Experimental Evaluation of a Fresnel Lens Solar Concentrator. NASA TM X-7333, August 1976.

5. Grimmer, D. and Herr, K.: Solar Process Heat from Concentrating Flat-Plate Collectors. Los Alamos Scientific Laboratory Report LA-6597-MS, December 1976.

6. Rohm and Haas Technical Data: PL-53h, Transmittance and Exposure Stability of Colorless Plexiglas Cast Sheet.

7. Rohm and Haas Technical Data: PL-165f, Plexiglas Acrylic Plastic Molding Powders.

8. Monsanto Company: Therminol Heat Transfer Fluids, a Design, Operating, and Maintenance Guide for Low-Cost, Low-Pressure Heat Transfer Systems. Technical Brochure IC/FF-33.

9. Ernst, L. and Rusk, R.: Solar Collector Test Facility. Sandia Laboratories Report SAND 74-0405, June 1975.

10. Seifert, W. F., et al: Design and Operational Consideration for High Temperature Organic Heat Transfer Systems. Process Heat Transfer Symposium of the 71st National AICHE Meeting, February 22-24, 1972.

11. Monsanto Company: Therminol 66. Technical Data Sheet IC/FF-35.

12. Cosby, R. M.: The Linear Fresnel Lens Solar Concentrator: Transverse Tracking Error Effects. Progress Report No. 2, Ball State University-Marshall Space Flight Center Cooperative Agreement, NCA8-00121, Modification No. 3, January 1977.

APPENDIX

OXIDE ABSORPTIVE COATING DEVELOPMENT

A. Application Survey Testing

Oxide coating application procedures and resulting optical properties were explored with and without nickel substrates, termed Process I and II, respectively. The Process I options investigated are shown in Figure A-1 and basically involve various development methods of preparing matt surface stainless steel before thermal oxidation at 900°C (1650°F). The resulting optical properties and comments are listed in Table A-1. Process IA was the least complicated procedure and consisted of heat treatment after degreasing and detergent cleaning. The coating produced was nonuniform in appearance with a maximum absorptance of 0.81 and minimum emittance of 0.1. The added step of acid cleaning in Process IB improved the coating uniformity, but the measured optical properties were basically unchanged. The optical properties were improved when the surface was electropolished before acid treatment (Process IC). A maximum absorptance of 0.89 and minimum emittance of 0.06 were obtained. Utilization of a bright dip chemical in Process ID resulted in properties slightly below those obtained with Process IC. Since use of the bright dip required more complex control procedures than those involved in Process IC, Process ID was not pursued further.

The effectiveness of the oxide type coating apparently varies with the stainless steel alloy. Preliminary testing was conducted with stainless steel alloys 302, 304, and 316 using Process I. The data listed in Table A-2 indicate that an improved coating resulted with 302 stainless using Processes IA and IB as a basis for the comparison. Since 304 stainless tubing was readily available at the time of receiver assembly fabrication, the oxide coating on 302 stainless was not pursued.

The Process II options explored are indicated by Figure A-2. Process IIA involved electroplating a 0.25 mil sulfamate nickel substrate and thermal oxidation at 455°C (850°F). Process IIB was the same except that bright nickel was the substrate. Table A-1 presents the Process II results. Poor substrate adhesion and inferior optical properties occurred with the bright dip nickel (Process IIB); whereas, the sulfamate nickel substrate provided a stable coating with slightly improved optical properties relative to Process I.

B. Final Application Procedures

Based on the above application survey testing and environment testing described below, Processes IC (stainless oxide) and IIA (nickel oxide) were developed into the final application procedures described in Tables A-3 and A-4, respectively. It was desired that the stainless and nickel oxide coating be tested via utilization in the Fresnel lens receiver assembly. However, only the stainless oxide was used on the current absorber tube because a chemical bath for nickel plating the full length tube was not available. Also because of chemical bath limitations, buffing the tube surface was utilized in lieu of electroplating in the stainless oxide application.

C. Environment Testing

The steel oxide and sulfamate nickel oxide coatings were subjected to humidity, salt spray, and UV exposure tests. No degradation of optical properties occurred during 18 months of exposure to 100 percent relative humidity at 35°C, nor during 250 equivalent Sun hours of UV exposure. The steel oxide tolerated approximately 4 hours of salt spray before visible pitting and coating degradation occurred; whereas, the sulfamate nickel oxide tolerated 4 weeks. The salt spray is a harsh environment, therefore, both coatings resist corrosion quite well, but the nickel oxide is definitely more resistant. The steel oxide was also subjected to 25 days of thermal cycling which consisted of maintaining a temperature of 540°C for 6 hours and, then, room temperature for 18 hours. No degradation occurred. Although the nickel oxide has not been subjected to thermal cycling tests, it is speculated that it is durable to the 370° to 430°C range on stainless steel base materials.
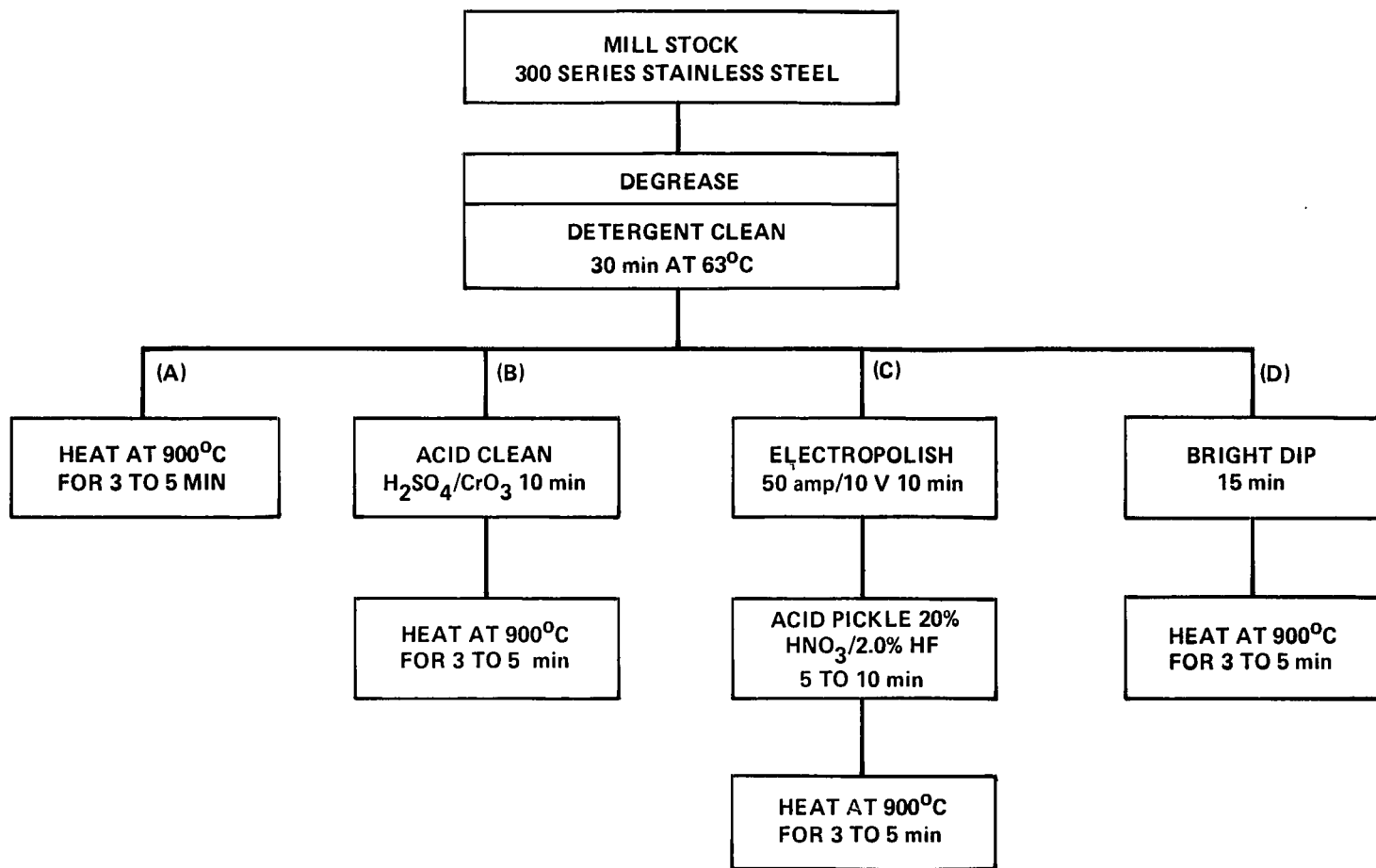
Figure A-1. Stainless oxide coating application options, Process I.

```
                    ┌─────────────────────────────┐
                    │         MILL STOCK          │
                    │  300 SERIES STAINLESS STEEL │
                    └─────────────────────────────┘
                                  │
                                  ▼
                    ┌─────────────────────────────┐
                    │          DEGREASE           │
                    ├─────────────────────────────┤
                    │      DETERGENT CLEAN        │
                    │      30 min AT 63°C         │
                    └─────────────────────────────┘
                                  │
         ┌────────────────────────┴────────────────────────┐
         ▼                                                  ▼
┌─────────────────────────────┐            ┌─────────────────────────────┐
│ ELECTROPLATE 0.25 Mil NICKEL│            │  ELECTROPLATE 0.25 mil      │
│ USING SULFAMATE NICKEL BATH │            │  BRIGHT NICKEL              │
│ 30 min                      │            │  15 min                     │
└─────────────────────────────┘            └─────────────────────────────┘
         │                                                  │
         ▼                                                  ▼
┌─────────────────────────────┐            ┌─────────────────────────────┐
│ ACID ETCH (HNO₃/HF)         │            │  ACID ETCH (HNO₃/HF)        │
│ 30 sec                      │            │  30 sec                     │
└─────────────────────────────┘            └─────────────────────────────┘
         │                                                  │
         ▼                                                  ▼
┌─────────────────────────────┐            ┌─────────────────────────────┐
│ THERMALLY OXIDIZE AT        │            │  THERMALLY OXIDIZE          │
│ 455°C FOR 3 min             │            │  AT 455°C FOR 3 min         │
└─────────────────────────────┘            └─────────────────────────────┘
```

MILL STOCK
300 SERIES STAINLESS STEEL

DEGREASE

DETERGENT CLEAN
30 min AT 63°C

ELECTROPLATE 0.25 Mil NICKEL
USING SULFAMATE NICKEL BATH
30 min

ELECTROPLATE 0.25 mil
BRIGHT NICKEL
15 min

ACID ETCH (HNO_3/HF)
30 sec

ACID ETCH (HNO_3/HF)
30 sec

THERMALLY OXIDIZE AT
455°C FOR 3 min

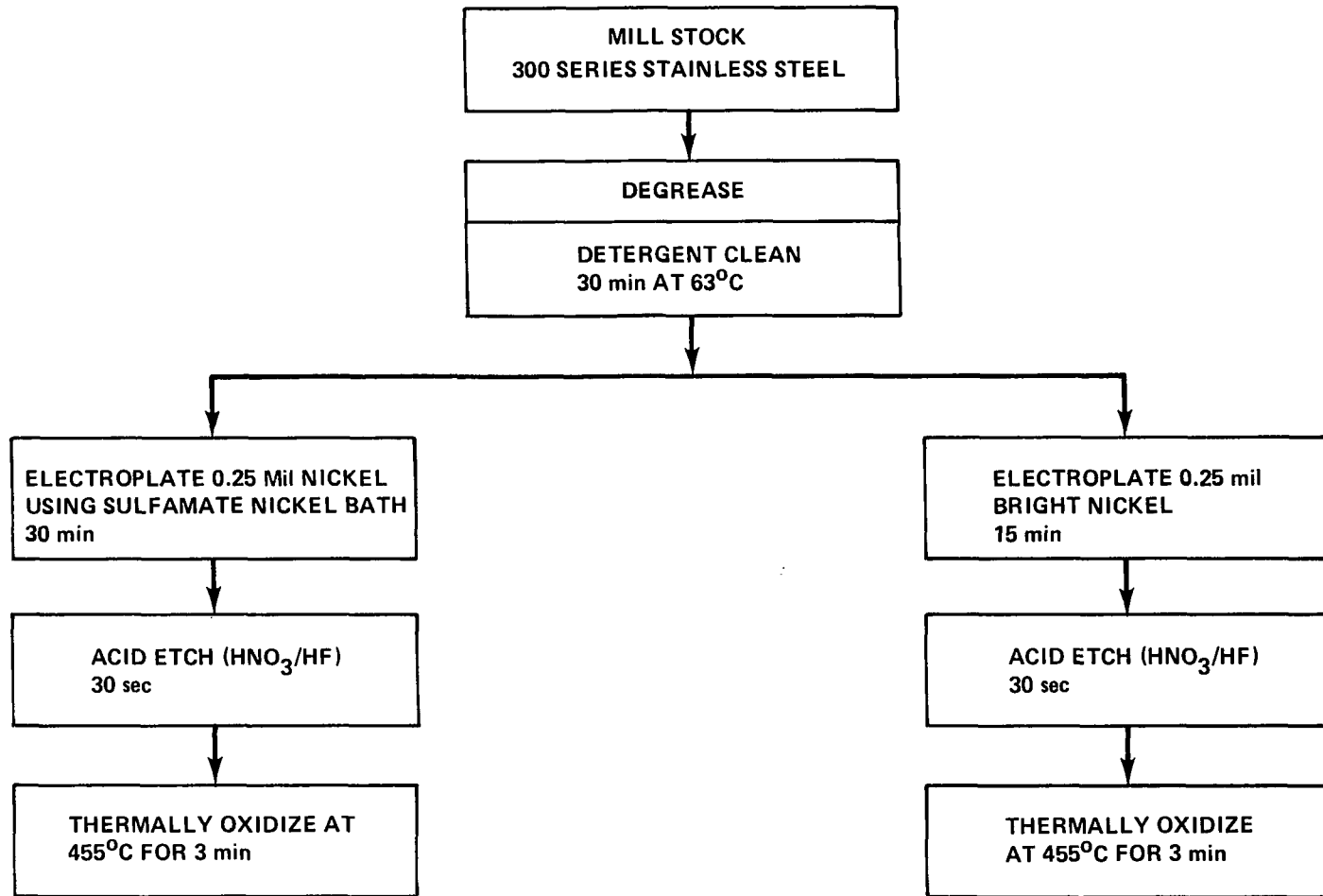THERMALLY OXIDIZE
AT 455°C FOR 3 min

Figure A-2. Nickel sulfamate coating application options, Process II.

TABLE A-1. ABSORPTIVE COATING OPTICAL PROPERTIES VERSUS APPLICATION PROCEDURE WITH 304 STAINLESS

Process	Type Oxide	Optical Properties	Comments
IA	Stainless Steel	$\alpha = 0.72 - 0.81$ $\epsilon = 0.10 - 0.21$ $\alpha/\epsilon = 4.8 - 7.6$	Nonuniform Appearance, Good Stability
IB	Stainless Steel	Same as Above	Improved Visual Uniformity, Good Stability
IC	Stainless Steel	$\alpha = 0.83 - 0.89$ $\epsilon = 0.06 - 0.08$ $\alpha/\epsilon = 13.8 - 11.1$	Improved Optical Properties, Good Stability
ID	Stainless Steel	$\alpha = 0.76 - 0.85$ $\epsilon = 0.096 - 0.15$ $\alpha/\epsilon = 5.1 - 8.9$	More Complicated Application Procedures; Process Refinement not Pursued as in IC
IIA	Sulfamate Nickel	$\alpha = 0.85 - 0.89$ $\epsilon = 0.05 - 0.08$ $\alpha/\epsilon = 14.3 - 28.3$	Post Plating Etch Eliminated By Process Refinement
IIB	Bright Nickel	$\alpha = 0.63 - 0.66$ $\epsilon = 0.04 - 0.05$ $\alpha/\epsilon = 13.0 - 16.5$	Unsatisfactory Optically, Poor Plating Adhesion Due to Brittle Nature of Electrodeposit

TABLE A-2. OXIDE COATING OPTICAL PROPERTIES VERSUS STAINLESS ALLOY

Type Alloy	Processes IA and IB	Process IC	Process ID
302	$\alpha = 0.78 - 0.87$ $\epsilon = 0.10 - 0.13$ $\alpha/\epsilon = 6.5 - 7.8$		
304L	$\alpha = 0.72 - 0.81$ $\epsilon = 0.10 - 0.21$ $\alpha/\epsilon = 4.8 - 7.6$	$\alpha = 0.83 - 0.89$ $\epsilon = 0.06 - 0.08$ $\alpha/\epsilon = 13.8 - 11.1$	$\alpha = 0.76 - 0.85$ $\epsilon = 0.096 - 0.15$ $\alpha/\epsilon = 5.1 - 8.9$
316L	$\alpha = 0.75 - 0.83$ $\epsilon = 0.69 - 0.25$ $\alpha/\epsilon = 1.1 - 3.2$	$\alpha = 0.84$ $\epsilon = 0.09$ $\alpha/\epsilon = 8.8$	

TABLE A-3. OXIDE COATING APPLICATION PROCEDURE FOR 304 STAINLESS TUBING

Step	Process	Chem/Equip	Concentration	Temperature	Time	Remarks
1.	Hand Wipe	Xylene		Ambient		
2.	Buff	Wire Wheel				Uniform surface texture
3.	Hand Wipe	Perchloroethylene		Ambient		
4.	Degrease	Perchloroethylene		121°C		
5.	Alkaline Soak	Turco 4215	12 ± 3 oz/gal	77°C	20 min	
6.	Hand Wipe	Turco 4215	12 ± 3 oz/gal	Ambient		
7.	Alkaline Soak	Turco 4215	12 ± 3 oz/gal	77°C	5 min	
8.	Rinse	DI H_2O		Ambient		
9.	Pickle	HNO_3 HF	30% 2%	Ambient	1 hr	
10.	Rinse	DI H_2O Hose		Ambient		Do not touch, surface easily contaminated.
11.	Blow Dry	Missile Grade Air		Ambient or Higher		
12.	Bag	Nylon Tube				Only inside of nylon bag should touch tube
13.	Oxidize Surface	Tube Furnace		900°C		Feed rate = 4.5 in./min/2 ft section

TABLE A-4. SULFAMATE NICKEL OXIDE COATING APPLICATION PROCEDURE FOR 304 STAINLESS TUBING

Step	Process	Chemical/ Material	Concentration	Tank* Number	Anode Material	Tank Lining	amp/ft^2	Temperature	Time (min)	Remarks
1.	Hand Clean	Acetone Wipe						Ambient		Thorough cleaning required
2.	Degrease	Perchloroethylene						121°C		Optional
3.	Rinse	DI H_2O		75				Ambient		
4.	Alkaline Soak	Altrex	8 oz/gal	74				60°C	5 to 10	
5.	Rinse	DI H_2O		75				Ambient		
6.	Electropolish	TMC	N/A	2	Stainless Steel	Stainless Steel	8 to 10 Volts	55° to 71°C	5 to 10	For surface metal removal
7.	Rinse	DI H_2O		1						
8.	Anodic Activate	H_3PO_4	75%	24	Lead	PVC	100	Ambient	1 to 2	
9.	Rinse	DI H_2O		25				Ambient		Thorough rinse
10.	Cathodic Activate	H_2SO_4	44%	26	Lead	PVC	100	Ambient	3 to 5	
11.	Rinse	DI H_2O		27				Ambient		
12.	Nickel Plate	$NiSO_4$ SNR	Ni – 76 gm/1 H_3BO_3 41 gm/1	30	Nickel	Poly Prop	20 to 25	49°C	30'	
13.	Rinse	DI H_2O		29				Ambient	15	Flush with DI H_2O Critical rinse
14.	Dry	Missile Grade Air						Ambient		
15.	Oxidation	Air		Furnace				510°C	4 to 5 0.020 in.	Time depends on sub. thick. 1/8 in. = 18 min.

*Tank Number designates the specific tanks used within the MSFC Materials and Processes Laboratory.

1. REPORT NO. NASA TP-1005	2. GOVERNMENT ACCESSION NO.	3. RECIPIENT'S CATALOG NO.
4 TITLE AND SUBTITLE An Analytical and Experimental Investigation of a 1.8 by 3.7 Meter Fresnel Lens Solar Concentrator		5. REPORT DATE August 1977
		6. PERFORMING ORGANIZATION CODE
7. AUTHOR(S) Leon J. Hastings, Steve L. Allums, and Warren S. Jensen		8. PERFORMING ORGANIZATION REPORT # M-224
9. PERFORMING ORGANIZATION NAME AND ADDRESS George C. Marshall Space Flight Center Marshall Space Flight Center, Alabama 35812		10. WORK UNIT NO.
		11. CONTRACT OR GRANT NO.
12. SPONSORING AGENCY NAME AND ADDRESS National Aeronautics and Space Administration Washington, D.C. 20546		13. TYPE OF REPORT & PERIOD COVERED Technical Paper
		14. SPONSORING AGENCY CODE

15. SUPPLEMENTARY NOTES

Prepared by Structures and Propulsion Laboratory, Science and Engineering

16. ABSTRACT

Line-focusing acrylic Fresnel lenses with application potential in the 200° to 370°C range are being analytically and experimentally evaluated. Investigations previously conducted with a 56 cm wide lens have been extended by the present study to experimentation/analyses with a 1.8 by 3.7 m lens. A measured peak concentration ratio of 64 with 90 percent of the transmitted energy focused into a 5.0 cm width was achieved. A peak concentration of 61 and a 90 percent target width of 4.5 cm were analytically computed. The experimental and analytical lens transmittance was 81 percent and 86 percent, respectively. Thus, the analytical/experimental lens performance correlation is considered good. The lens also was interfaced with a receiver assembly and operated in the collection mode. The collection efficiency ranged from 42 percent at 100°C to 26 percent at 300°C, whereas an efficiency of 40 percent at 300°C was anticipated. Apparently, the reflective cavity surrounding the absorber tube did not perform as expected. Therefore, future receiver assemblies will decrease or eliminate reliance on reflective surfaces, i.e., the energy focused directly on the absorber tube surfaces will be increased. Efficiency improvements to the 40 to 50 percent range are anticipated.

EDITOR'S NOTE

17. KEY WORDS	18. DISTRIBUTION STATEMENT STAR Category 44

19. SECURITY CLASSIF. (of this report) Unclassified	20. SECURITY CLASSIF. (of this page) Unclassified	21. NO. OF PAGES 75	22. PRICE $4.50

*For sale by the National Technical Information Service, Springfield, Virginia 22161.

507 001 C1 U   E 770708 S00903DS
DEPT OF THE AIR FORCE
AF WEAPONS LABORATORY
ATTN: TECHNICAL LIBRARY (SUL)
KIRTLAND AFB NM 87117

NASA

POSTMASTER :   If Undeliverable (Section 158
                Postal Manual) Do Not Return